M.A. AL IMRAN

ENHANCED MULTIPATH-BASED LOCALIZATION OF RADARS USING MACHINE LEARNING

THE GRADUATE SCHOOL OF NATURAL AND APPLIED SCIENCES
OF
ATILIM UNIVERSITY

MD ABDULLAH AL IMRAN

A DOCTOR OF PHILOSOPHY THESIS
IN
THE DEPARTMENT OF ELECTRICAL AND ELECTRONICS ENGINEERING

JANUARY 2024

ATILIM UNIVERSITY 2024

ENHANCED MULTIPATH-BASED LOCALIZATION OF RADARS USING MACHINE LEARNING

A THESIS SUBMITTED TO
THE GRADUATE SCHOOL OF NATURAL AND APPLIED SCIENCES
OF
ATILIM UNIVERSITY

BY

MD ABDULLAH AL IMRAN

IN PARTIAL FULFILLMENT OF THE REQUIREMENTS
FOR
THE DEGREE OF DOCTOR OF PHILOSOPHY
IN
ELECTRICAL AND ELECTRONICS ENGINEERING

JANUARY 2024

Approval of the Graduate School of Natural and Applied Sciences, Atilim University.

Prof. Dr. Ender KESKİNKILIÇ
Director

I certify that this thesis satisfies all the requirements as a thesis for the degree of **Doctor of Philosophy in Electrical and Electronics Engineering Department, Atilim University**.

Prof. Dr. Reşat Özgür DORUK
Head of Department

This is to certify that we have read the thesis Enhanced Multipath-based Localization of Radars using Machine Learning submitted by MD ABDULLAH AL IMRAN and that in our opinion it is fully adequate, in scope and quality, as a thesis for the degree of Doctor of Philosophy.

Prof. Dr. Ali KARA
Co-Supervisor

Assoc. Prof. Dr. Yaser DALVEREN
Supervisor

Examining Committee Members:

Prof. Dr. Ayhan ALTINTAŞ
Electrical and Electronics Eng., Bilkent University

Assoc. Prof. Dr. Yaser DALVEREN
Electrical and Electronics Eng., Atilim University

Prof. Dr. Mehmet ÇİYDEM
Electrical and Electronics Eng., Gazi University

Prof. Dr. Reşat Özgür DORUK
Electrical and Electronics Eng., Atilim University

Assoc. Prof. Dr. Beytullah YILDIZ
Software Engineering, Atilim University

Date: January 22, 2023

I declare and guarantee that all data, knowledge and information in this document has been obtained, processed and presented in accordance with academic rules and ethical conduct. Based on these rules and conduct, I have fully cited and referenced all material and results that are not original to this work.

Name, Last Name : MD ABDULLAH AL IMRAN

Signature :

ABSTRACT

Enhanced Multipath-based Localization of Radars using Machine Learning

Al Imran, Md Abdullah

Ph.D., Department of Electrical and Electronics Engineering

Supervisor : Assoc. Prof. Dr. Yaser DALVEREN

Co-Supervisor : Prof. Dr. Ali KARA

January 2024, 76 pages

The purpose of this thesis is to assess the reliability of a proposed approach for the passive localization of radar emitters in Electronic Support Measures (ESM) systems, specifically amidst uneven landscapes, employing a single receiver. The absence of empirical evidence regarding the accuracy of this method when applied to real data obtained from realistic scenarios raises a genuine concern in practical settings. To address this, an accurate ray tracing (RT) algorithm is employed to enable the implementation of the method in practice. Realistic scenarios are then established by utilizing a geographic information system (GIS) map, which aids in the collection of high-resolution digital terrain elevation data (DTED) and the consideration of realistic localization challenges associated with radar emitters. Subsequent simulations are conducted to assess the efficacy of the localization method. As a result, the performance of the method is validated for its practical implementation in the context of Electronic Warfare (EW), marking a significant milestone. Due to inherent characteristics of the method employed, the proposed approach suffers from computational complexity. In an effort to boost computational efficiency, a Machine Learning (ML)-based approach is introduced for the proposed method. The suggested ML framework requires useful features like Path Loss, Geometric Dilution of Precision (GDOP) of the sensor group and a performance metric namely Mean Square Error (MSE) obtained from the

priori-known operational environment. Since the performance of such a data-driven approach depends on the breadth of the dataset, a novel technique is developed to generate pseudo-realistic terrain view models motivated from the Aegean Sea islands. Three ML models: Stepwise Linear Regression, Decision Tree, and Neural Networks were trained, and tested on the datasets to predict the most optimal sensor groups to be used in a localization algorithm. Based on the results, it has been observed that the Decision Tree model is able to reach the highest prediction accuracy. Furthermore, the performance of the proposed approach was evaluated in terms of localization accuracy and computational speed. Apart from MSE, Circular Error Probable (CEP), and Spherical Error Probable (SEP) were also used to evaluate the estimation accuracy. From the achieved results, it has been concluded that the proposed approach is computationally efficient and applicable in the EW context, on the condition that the operational environment is known prior to implementation.

Keywords: ESM, GDOP, Machine Learning, Multipath Localization, Ray Tracing

ÖZ

Makine Öğrenmesi Kullanılarak Geliştirilmiş Çok Yollu Yayılım Yöntemiyle Radarların Konumlandırılması

Al Imran, Md Abdullah

Doktora, Elektrik ve Elektronik Mühendisliği

Tez Yöneticisi : Doç. Dr. Yaser DALVEREN

Ortak Tez Yöneticisi : Prof. Dr. Ali KARA

Ocak 2024, 76 sayfa

Bu tezin amacı, Elektronik Destek Tedbirleri (ESM) sistemlerinde, özellikle engebeli arazilerde, tek bir alıcı kullanarak radar yayıcılarının pasif olarak konumlandırılması için önerilen bir yaklaşımın uygulanabilirliğini değerlendirmektir. Gerçekçi senaryolardan elde edilen gerçek verilere uygulandığında bu yöntemin doğruluğuna ilişkin ampirik kanıtların olmaması, pratik ortamlarda gerçek bir endişe yaratmaktadır. Bunu ele almak için, yöntemin pratikte uygulanmasını sağlamak üzere isabetli bir ışın izleme (RT) algoritması kullanılmaktadır. Daha sonra, yüksek çözünürlüklü sayısal arazi yükseklik verilerinin (DTED) toplanmasına ve radar yayıcılarıyla ilişkili gerçekçi lokalizasyon zorluklarının dikkate alınmasına yardımcı olan bir coğrafi bilgi sistemi (GIS) haritası kullanılarak gerçekçi senaryolar oluşturulmuştur. Daha sonra, yerelleştirme yönteminin etkinliğini değerlendirmek için simülasyonlar gerçekleştirilmiştir. Sonuç olarak, yöntemin performansı Elektronik Harp (EH) bağlamında pratik uygulaması için doğrulanarak önemli bir dönüm noktasına ulaşılmıştır. Kullanılan yöntemin doğal özellikleri nedeniyle, önerilen yaklaşım hesaplama karmaşıklığından muzdariptir. Hesaplama verimliliğini artırmak amacıyla, önerilen yöntem için Makine Öğrenimi (ML) tabanlı bir yaklaşım getirilmiştir. Önerilen ML çerçevesi önceden bilinen operasyonel

ortamdan elde edilen Yol Kaybı, sensör grubunun Geometrik Hassasiyet Seyreltmesi (GDOP), ve Ortalama Kare Hata (MSE) performans ölçütü gibi faydalı özellikler gerektirir. Bu tür veri odaklı bir yaklaşımın performansı veri kümesinin genişliğine bağlı olduğundan, Ege Denizi adalarından motive edilmiş sözde gerçekçi arazi görünümü modelleri oluşturmak için özgün bir teknik geliştirilmiştir. Üç makine öğrenimi modeli: Kademeli Doğrusal Regresyon, Karar Ağacı ve Sinir Ağları eğitilmiş ve bir lokalizasyon algoritmasında kullanılacak en uygun sensör gruplarını tahmin etmek için veri kümeleri üzerinde test edilmiştir. Sonuçlara göre, Karar Ağacı modelinin en yüksek tahmin doğruluğuna ulaşabildiği görülmüştür. Ayrıca, önerilen yaklaşımın performansı lokalizasyon doğruluğu ve hesaplama hızı açısından değerlendirilmiştir. Kestirim doğruluğunu değerlendirmek için MSE'nin yanı sıra Dairesel Hata Olasılığı (CEP) ve Küresel Hata Olasılığı (SEP) da kullanılmıştır. Elde edilen sonuçlardan, önerilen yaklaşımın hesaplama açısından verimli olduğu ve uygulama öncesinde operasyonel ortamın bilinmesi koşuluyla EH bağlamında uygulanabilir olduğu sonucuna varılmıştır.

Anahtar Kelimeler: EDT, GDOP, Makine Öğrenmesi, Çokyollu Lokalizasyon, Işın İzleme

To

My Mother,
The unsung and anonymous hero in my life.
For being my first and foremost teacher. And the unconditional shower of love and support.

My Father,
A strong and gentle soul.
For the unheralded sacrifices, relentless encouragements and being a dad.

My Siblings,
For believing in me even when I didn't have the courage to and tolerating my endless mischievousness.

ACKNOWLEDGMENTS

I would like to express immense gratitude to my supervisors Prof. Dr. Ali KARA and Assoc. Prof. Dr. Yaser DALVEREN, who facilitated this rough journey with their solution-oriented approach.

I shall also thank my close friends and family members for making this adventure colorful and their emotional support.

Furthermore, I thank all the members of the Department of Electrical and Electronics Engineering of Atilim University for helping me throughout the dissertation phase. Lastly, I am grateful to Assoc. Prof. Dr. Mehmet Barış TABAKCIOĞLU for supplying me with a hardware platform to run month-long tests.

This work was funded by *The Scientific and Technical Research Council of Turkey (TÜBİTAK)* under the National Support Programmes code #1001.

TABLE OF CONTENTS

LIST OF TABLES

TABLES

LIST OF FIGURES

FIGURES

LIST OF SYMBOLS

AOA	:	Angle of Arrival
CEP	:	Circular Error Probable
CIR	:	Channel Impulse Response
DTED	:	Digital Terrain Elevation Data
ESM	:	Electronic Support Measures
EW	:	Electronic Warfare
FDOA	:	Frequency Difference of Arrival
GDOP	:	Geographic Dilution of Precision
GIS	:	Geographic Information System
LOP	:	Line of Position
LOS	:	Line of Sight
ML	:	Machine Learning
MSE	:	Mean Square Error
NLS	:	Nonlinear Least-Squares
PL	:	Path Loss
RD	:	Range Difference
RF	:	Radio Frequency
RMSE	:	Root Mean Square Error
RT	:	Ray Tracing
SEP	:	Spherical Error Probable
TDOA	:	Time Difference of Arrival
TOA	:	Time of Arrival
eAOA	:	Error in Angle of Arrival

CHAPTER 1

INTRODUCTION

The impact and importance of positioning is so widespread and popular that oftentimes the term emitter localization is synonymously used for the radar system itself. In other words, it is a fundamental aspect of radio engineering that still is profusely relevant to the present days. Emitter localization is of utmost importance for numerous applications ranging from civil, military, space, air traffic control, healthcare, defense, military, logistics, warehousing, data-context and more [1–7].

Although location estimation often refers to active transmitter positioning [8–12], where the bearing information contained signal radiated or reflected from an object is utilized in an observing array, passive forms of localization techniques have seen a rising interest in the recent years [13–19].

1.1 Motivation

Over the years, the passive localization of radar emitters has been of great interest in a wide range of applications, such as electronic warfare (EW). One of the important benefits of passive localization systems over active localization is their cost efficiency in determining the position of the emitter. Particularly when the complex nature of the electromagnetic environment is concerned, the importance of a passive localization system becomes more evident. In a conventional passive localization system, the emitter's position is determined by utilizing measurements obtained from multiple sensors, also known as receivers. Therefore, depending on the type of receiver measurements, numerous localization algorithms were proposed to be used in a typical passive localization system. The widely recognized algorithms [20] primarily rely on

the utilization of the angle of arrival (AOA), time of arrival (TOA), and time difference of arrival (TDOA) measurements [21–23]. Moreover, in recent years, machine learning (ML) has begun to be applied to localization systems in order to improve their effectiveness [13, 24–26].

In real-world applications, the flaws caused by outdoor multipath propagation are considered a significant obstruction to the accurate implementation of localization algorithms. Multipath scattering originates from stationary or moving objects in the environment that combine with the direct signals emitted from the target, reducing the performance of the localization algorithms. One of the ways to improve localization accuracy is to mitigate the multipath effects [27, 28]. An alternative method entails capitalizing on the multipath phenomena to determine the location of emitters by employing either multiple receivers [29–31] or a single receiver [32–39]. Localization algorithms that utilize multipath exploitation in single-receiver emitter systems present notable benefits, such as improved localization accuracy and reduced expenses associated with system deployment. Thus, exploiting the indirect propagation paths in emitter localization using a single receiver is still a popular research direction to overcome operational challenges expected in real-world applications in terms of robustness and effectiveness.

The majority of research in the field of emitter localization methods, which rely on exploiting multipath signals, has primarily targeted indoor or urban applications. In these methods, only specular reflection was employed in order to exploit multipath. The development of a method for localizing a single-receiver emitter in the presence of irregular terrain using diffuse scattering and multipath exploitation for electronic warfare (EW) applications has received minimal attention in the existing body of research. One of the works within this context is presented in [38], where only the theoretical development of a localization method is introduced. The method employed in this thesis relied on the utilization of multipath scattering centers as virtual sensors, along with the integration of Geographical Information System (GIS) and Ray Tracing (RT) algorithm. It is worth mentioning that the probability of these scattering centers serving as sources of multipath signals can be determined by calculating the Path Loss (PL) for the specific links connecting the radar transmitter and the receiver. Consequently, to estimate the location of the radar source, a weighted averaging

approach was suggested, which combines the results obtained from the GIS-assisted RT algorithm and a Time Difference of Arrival (TDOA) technique. In [39], an evaluation was conducted to assess the precision of the approach suggested in [38] using real data obtained from practical scenarios. This thesis serves as a continuation of the previous research, aiming to validate the effectiveness of the method in real-world conditions. To this end, the Digital Terrain Elevation Data (DTED) collected from a 3D GIS map was used in an RT algorithm. Based on the simulation findings, it was determined that while the proposed method demonstrates satisfactory accuracy in practical situations, its computational complexity remains a significant limitation. Furthermore, it was emphasized that the precision of localization is contingent upon the placement of the sensors. In other words, the accuracy is expected to be degraded under poor virtual sensor geometry, so-called the large Geometric Dilution of Precision (GDOP). Thus, the GDOP can be utilized as a useful criterion to enhance the efficiency of the localization method.

In general, target localization in a single-receiver setup in multipath environments is expected to be a challenging task when the nature of the problem is complex. Because of this complexity, the relevance and size of a dataset, including the measurements from the multipath environment, could be considered significant concerns. Thus, it might be very difficult to formulate or solve the problem with straightforward mathematical methods in a simple way. Recently, it has been proposed in a study that ML can be applied in order to overcome such issues [40]. In this thesis, a combination of a ray-tracing simulation tool and a kernel-based machine learning framework is adopted to localize Radio Frequency (RF) emitters using a single sensor. The hybrid approach involves extracting the multipath fingerprint through the ray-tracing simulation tool, while relying exclusively on the signal reflections from the building walls in the proposed methodology. This makes the proposed approach applicable for improving RF emitter localization performance in urban settings. Nevertheless, integrating ML into single-receiver localization systems is one of the most promising approaches to mitigate the challenges with respect to both accuracy and complexity in multipath environments.

1.2 Purpose and Contribution

This research is dedicated to addressing the apprehensions associated with the effectiveness of the localization technique suggested in [38] in practical situations, as depicted in Figure 1.1. Here, the emitter source is illustrated on the open-wide sea whereas the passively-listening intercept receiver is shown surrounded by the irregular terrain. In order to achieve this objective, an initial step involves adapting an RT algorithm through the utilization of reasonable obstruction models. Hence, realistic scenarios are created in specific areas (e.g. the Mykonos Islands) of the Aegean Sea. Subsequently, a GIS map is synthesized from each scenario to gather the elevation data. Then, the RT algorithm employs these data to determine the probability of the scattering regions serving as a multipath source. Additionally, the identified multipath scattering centers can be used as virtual sensors for the purpose of an efficient TDOA-based localization method, known as improved two-step weighted least-squares (improved-TSWLS) [41]. To incorporate all virtual sensors and their likelihoods in the location estimation process, a weighted averaging technique is implemented. Following this, simulations are conducted to assess the feasibility and validity of the proposed method within realistic scenarios. Consequently, the performance limits of the method in such scenarios are thoroughly examined and documented.

Furthermore, the author proposes a ML-based approach that can be used as a low computational cost alternative to the radar emitter localization method presented in [39]. The idea is to use a ML model on a dataset, including the useful features obtained from the priori-known operational environment. One of the features is the PL value of the emitter-scattering center (virtual sensor)-receiver links. Another feature is the GDOP value that can be calculated for individual virtual sensor groups. The last feature is the Mean Square Errors (MSEs) of the position estimates acquired by [39]. Thus, after training an ML model on the created dataset, it can be expected that a virtual sensor group with the potential to provide an optimal location estimate in terms of low MSE could be obtained. This virtual sensor group is then proposed to be used in one of the efficient localization algorithms based on TDOA measurements in order to estimate the location of the radar emitter.

In order to verify the applicability and computational efficiency of the approach

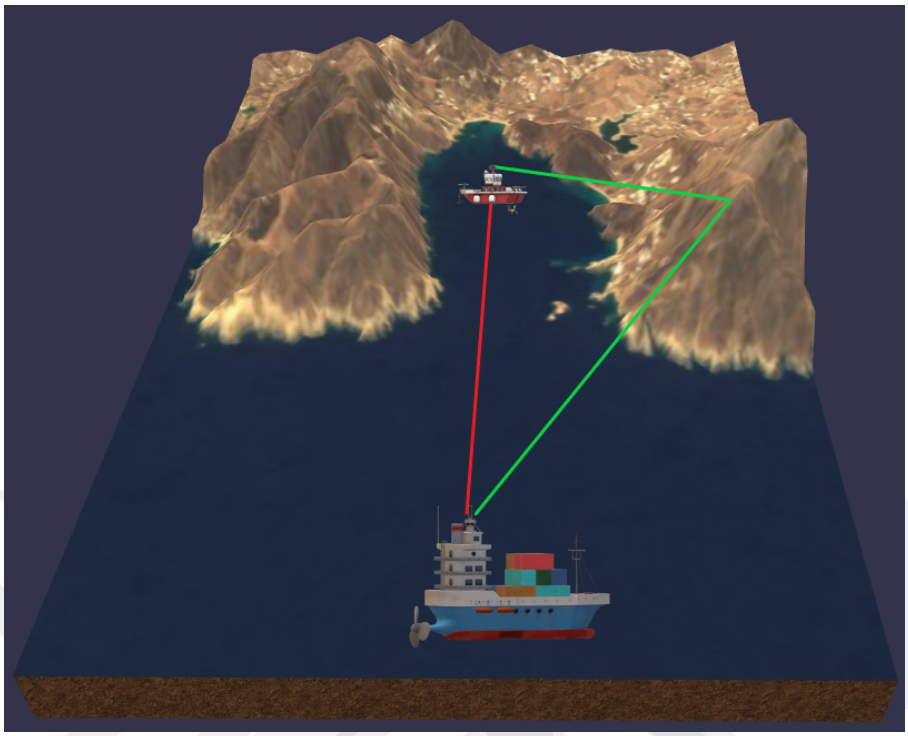

Figure 1.1: Realistic Deployment Scenario in 3D.

presented in this thesis, realistic scenario-based experiments were conducted. In this context, datasets that consist of a huge amount of data collected from realistic scenarios were created. To create such datasets, first, a specific 3D region of the Aegean Sea was selected. Then, the GIS map of the region was generated. To gather the necessary data, it was imperative to alter the topographical characteristics of the area. Therefore, the terrain profile of the region was reproduced by generating pseudo-realistic terrain views (models). In this way, unique localization scenes were achieved under various realistic scenarios, each of which was defined by the radar beamwidth, the receiver placement, and the radar emitter-receiver distance. Next, simulations were performed on the pseudo-realistic scenes to create the dataset containing positional MSE estimates and the GDOP along with the PL values. Since the features in the created dataset are well suited for the regression analysis, well-known ML models for regression, such as Stepwise Linear Regression, Regression (Decision) Tree, and Neural Networks (NNs), were trained and tested on the created datasets to predict the most optimal virtual sensor groups that enable to achieve the lowest MSEs of the

location estimates. The preliminary findings indicated that the Decision Tree model achieved the highest level of prediction accuracy when considering the Root Mean Squared Error (RMSE). Thereafter, the most optimal virtual sensor groups for each scenario predicted by the Decision Tree model were used in an accurate TDOA-based localization algorithm [41] to estimate the location of the radar emitter. Next, an extensive performance evaluation of the proposed approach and the method presented in [39] was provided based on their respective localization accuracy in the form of multiple metrics and computational speed. Through the analysis of the results, it was verified that the proposed approach is computationally efficient and applicable in the EW context, provided that the operational environment is known.

The scientific work presented herein has made significant contributions in the followings:

1. An accurate RT algorithm is utilized in a TDOA-AOA based localization method to fully develop a radar emitter localization technique.
2. Realistic localization problems for radar emitters are considered in the development of scenarios, using high-definition GIS data, ensuring its practical aspects for EW applications.
3. GDOP-assisted emitter localization in multipath exploiting single-receiver scenarios.
4. Adoption of Machine Learning techniques to lower the computational requirements in terms of localization speed and simultaneously increasing the estimation accuracy.
5. Novel data collection approach for multipath operational environments where DTED level 2 resolution pseudo-realistic terrains were employed.

The subsequent sections of this manuscript are structured as follows: Section 2 provides a concise overview of the localization method proposed in [39], along with a discussion on its computational complexity. This is followed by Section 3, where firstly experiments were conducted to assess the operational environment and deployment configurations. Then, based on the outcomes of the first part, a data-driven passive

single-receiver location estimation method is proposed, tested, and evaluated in terms of localization accuracy gains and computational efficiency. Section 4 presents some EW industry-standard performance metrics for extensive analysis of the proposed methods. This is followed by the conclusion in Section 5. Finally, future research directions and possible drawbacks and/or improvements are discussed in Section 6.

CHAPTER 2

LITERATURE REVIEW & PROBLEM STATEMENT

This section commences with a description of the localization method outlined in [39] before introducing our proposed approach. Following that, we delve into the issue of computational complexity that arises with the localization method.

2.1 Related Works

2.1.1 Classic Localization Approach

One of the studies available in the literature is presented in [31], which focuses on solving a localization problem in the presence of multipath interference. In this scenario, the signal emitted by a source undergoes reflections from a surface. The authors propose a particle-filtering algorithm that utilizes Angle of Arrival (AOA) and Time Difference of Arrival (TDOA) measurements to estimate the location of the emitting source. In a different study, [42], the authors use a stationary receiver along with specular reflections from building interior walls to track and locate a mobile target. The study demonstrates that accurate localization in indoor environments can be designed by employing tracking algorithms with optional association of data. Another work, described in [32], introduces a Time of Arrival (TOA)-based algorithm for associating multipath reflections with their corresponding walls in urban sensing and through-the-wall (TTW) radar position estimation. The authors also develop a nonlinear least-squares (NLS) approach to mitigate propagation effects and improve localization accuracy. However, it should be noted that this algorithm assumes that the reflectors' characteristics are known. To address the requirement of resolving all

multipath components, [33] proposes an alternative approach. This approach utilizes embedded directivity in ultra-wideband antennas to relax the condition of resolving all multipath components, thereby achieving more flexible and accurate localization.

The given approach utilizes the dependence of pulse waveform on the direction of arrival (DOA) of the radar echo. Consequently, it is demonstrated that having a single-reflection component in conjunction with the radar echo is adequate for approximating the source location. In a study by O'Connor et al. [34], a technique is proposed for locating a source in urban environments by exploiting multipath. It is demonstrated that source localization in a three-dimensional volume, with a known waveform, can be attained with as low as five time of arrival (TOA) readings. Another research work by Giacometti et al. [35] focuses on utilizing angle of arrival (AOA) and time difference of arrival (TDOA) measurements to localize a radar emitter in a naval context, without any prior knowledge of the reflector locations. To address this problem, they propose an assignment algorithm-based method. In a study by Samizadeh et al. [36], the direct and scattered signals reaching two receivers are analyzed to localize the target where scatterer objects are prominent. The study presented in [43] suggests a technique that combines channel impulse response (CIR) approximation and RT simulation. In this method, the RT simulation tool is used to map the positions of the scatterers, providing valuable information about the ray paths. This information, along with time delay estimation, is then utilized to determine the location of an emitter in non-line-of-sight (NLoS) environments.

To summarize, the pertinent studies can be found in Table 2.1. It is evident from Table 2.1 that the majority of these studies utilize specular reflection exclusively to harness the benefits of multipath propagation. Furthermore, these studies primarily focus on applications within indoor or urban settings.

In contrast, the research presented in [38] is the only work that explores an advanced localization system within the domain of electronic warfare (EW). The study introduces a new approach for passively localizing radar emitters in electronic support measures (ESM) systems, specifically in irregular terrains. Unlike previous works, this approach incorporates the utilization of diffuse scattering over irregular terrain in multipath exploitation. The scattered regions over the irregular terrain, where the multipath

Table 2.1: Summary of single-receiver emitter localization works using multipath.

Ref.	Signal	Application	Multipath Component	Location Estimation Approach
[31]	TDOA & AOA	Multipath environments	Reflection	Particle-filtering algorithm
[32]	TOA	Indoor and TTW radar	Reflection	TOA wall association algorithm & NLS
[33]	TOA & DOA	Indoor and TTW radar	Reflection	Pulse waveform dependency on DOA of the radar echo
[34]	TOA	Indoor environment	Reflection	The Bancroft technique
[35]	TDOA & AOA	Naval context	Reflection	Assignment algorithm
[36]	TDOA & DOA	Easily modelable environment	Scattering	Electromagnetic modeling
[38]	TOA & AOA	ESM systems	Diffuse scattering	Weighted averaging based GIS-assisted TDOA technique
[42]	TOA	Indoor environment	Reflection	Tracking with optional data association
[43]	TDOA	NLoS environments	Diffraction and Reflection	RT simulation and CIR Combination

signals are scattered, are treated as virtual sensors in this approach. Additionally, the probability of these scattering regions contribution to multipath is assessed. To achieve this, a geographic information system (GIS) is combined with an RT algorithm. Consequently, a weighted averaging method, which employs both the GIS-assisted RT algorithm and a time difference of arrival (TDOA) technique, is employed to determine the emitter's location. It is important to note that the accuracy of localization is dependent on the identification of the likelihoods of the multipath scattered signals. Therefore, an accurate RT algorithm is necessary for calculating these likelihoods. That said, the research does not put forward a specific RT algorithm as it solely deliberates on the analytic conception of the localization method. Consequently, there are remains yet to be addressed factors regarding the position estimation accuracy of the suggested method practical use cases. Hence, it is imperative to improve the suggested approach by integrating an appropriate RT algorithm and assessing localization precision and efficiency in diverse practical situations.

2.1.2 Machine Learning Approaches

Conventional TDOA-based localization techniques suffer from the nonlinear optimization problem and hyperbolic intersection in estimation. The increasing complexity of real-life deployment environments, the disturbances of noise, perturbations and multipath phenomena further limits the performance of classical TDOA algorithms. Not to mention that the quality of TDOA measurements significantly influences the localization accuracy. Nonetheless, we restrict our focus on exploitation of multipath in complex NLOS-rich real environments where the traditional TDOA-based localization precision generally is insufficient and resource intensive.

The multipath phenomena, often considered a limitation, has seen quite some research interests [44–70]. These works can be categorized into (a) multipath mitigation, and (b) multipath exploitation to alleviate the positioning inaccuracy. The former classifies the multipath signals as outliers of the TDOA-based localization process whereas the latter, as the name suggests, aims to utilize the multipath information to gather further insight about the localization system and thus increase its accuracy. ML-based solutions have garnered considerable interest as a result of their exceptional performance and strong

modeling capabilities [71].

ML has emerged as a powerful framework for addressing numerous challenging practical issues across diverse domains. These domains encompass tasks such as image recognition, language translation, wireless transmission scheduling, and autonomous driving. In essence, ML leverages real-world data to train a solution that can comprehend the intricate relationships between input data (features) and output values (labels), which would otherwise be incomprehensible or even unattainable for humans. There also exists unsupervised ML where the data has no labels and the aim is to classify the data. Similarly, the localization aspect has seen quite some research interests and [72–79] are evident indications of such.

Literature has seen vast amount of research interests regarding localization and researchers are still working on novel techniques to improve localization performance. Here, we will focus only on the TDOA based multipath exploiting localization works. The most natural form of localization implies explicit coordination estimation and is relatively computationally heavy. Although, localization can be synonymously interchanged for classification and fingerprinting. Furthermore, we are concerned with the passive form of localization instead of the emitter being active or cooperative. Although localization services can be principally categorized into two: indoor and outdoor localization, we make no distinction here while screening the literature for relevant works. Nevertheless, the literature has seen a large share of researches directed towards the indoor localization techniques due to emerging technologies like WSN and 5G, and controllable environment aspects as opposed to outdoors case.

The related works regarding multipath employing TDOA-based localization methods can be summarized as of Table 2.2. The work presented at [80] identifies the multipath signals using Support Vector Machine (SVM) for TDOA-based indoor localization. This is a classification type of localization that discards the multipath signals to improve the positioning accuracy. Similarly, fingerprinting maps target to the closest known recorded location in the database. The accuracy of localization is determined by the resolution or separation of these fingerprints, as the classification performance relies on the quantity of classes or reference points. The works [81–86] are examples of fingerprinting. Here, [81, 82, 84] utilizes Random Forest and [83] employs Kernel

Table 2.2: Summary of ML-based single-receiver emitter localization works using multipath.

Ref.	Signal Feature	Multipath Approach	Method
[80]	TDOA	Multipath rejection in indoor	SVM
[81–84]	TDOA	Multipath rejection in outdoor using 2.4 GHz OFDM signal	Random Forest, Kernel
[85]	TDOA, RSS	Multipath to filter RSS in Indoor using LTE	Neural Network
[86]	TDOA	Multipath rejection in outdoor using LoRa	Neural Network, Random Forest
[87]	TDOA	Multipath mitigation in indoor using WiFi	Convolutional Neural Network
[88]	TDOA	Multipath mitigation for a simulated environment	Kalman Filter
[89]	TDOA, AOA	Multipath exploitation for UAV localization in urban scenario	Semidefinite Programming
[90]	TDOA, AOA	Multipath exploitation in the naval context	Kernel

to reject multipath in an outdoor environment while using 2.4 GHz OFDM signals. Multipath information is utilized to filter the Received Signal Strength (RSS) or path loss while using a Neural Network model for an indoor LTE application in [85]. A TDOA-based multipath rejection work for outdoor is presented in [86] that employs Neural Network and Random Forest. On the contrary, relevant coordination estimation works addressing some form of multipath are listed in [87–90]. Although deep convolutional neural networks (CNN) are typically used for image classification applications, [87] uses CNN to mitigate the impact of multipath for indoor Wi-Fi based positioning. Traditional iterative approaches like Kalman filter [88] and convex optimization problems like Semidefinite Programming (SDP) [89] are also proposed in the literature. TDOA along with AOA is employed in [89] to exploit the multipath effects for UAV localization. Lastly, [90] which also uses TDOA and AOA for multipath utilization in a hypothetical tactical scenario for naval applications using Kernel.

2.2 Fundamentals of the Localization Approach

The focus of this article is on the operational obstacles faced by ESM systems when determining the position of radar emitters for naval applications. More specifically, the presence of multipath signals with radar parameters similar to the radar beam area poses challenges for ESM systems in accurately identifying the radar emitter. Consequently, this issue significantly hampers the localization performance. In order to provide a clear comprehension of the problem, Figure 2.1 illustrates a simplified two-dimensional (2D) problem space (top-view), disregarding altitudes.

Figure 2.1 illustrates the positions of the radar target and ESM intercepter, denoted as $\mathbf{u}^o = [x^o, y^o, z^o]^T$ and $\mathbf{s}_0^o = [x_0^o, y_0^o, z_0^o]^T$, respectively. The brown irregular shapes in the figure represent the irregular terrains. To simplify the analysis, the consideration is limited to two propagation paths: the direct path and a multipath. A generic TDOA pulses' diagram is depicted in Figure 2.2, where the direct pulse is received with a delay of t_D and multipath signals arriving from reflector region A after t_{A1} times, and so on. Notice how the signal strength decreases over time and distance traveled. To address the problem of localizing an emitter from a single receiver using direct and multipath pulses, a novel method is being sought after [38]. The primary purpose is to exploit

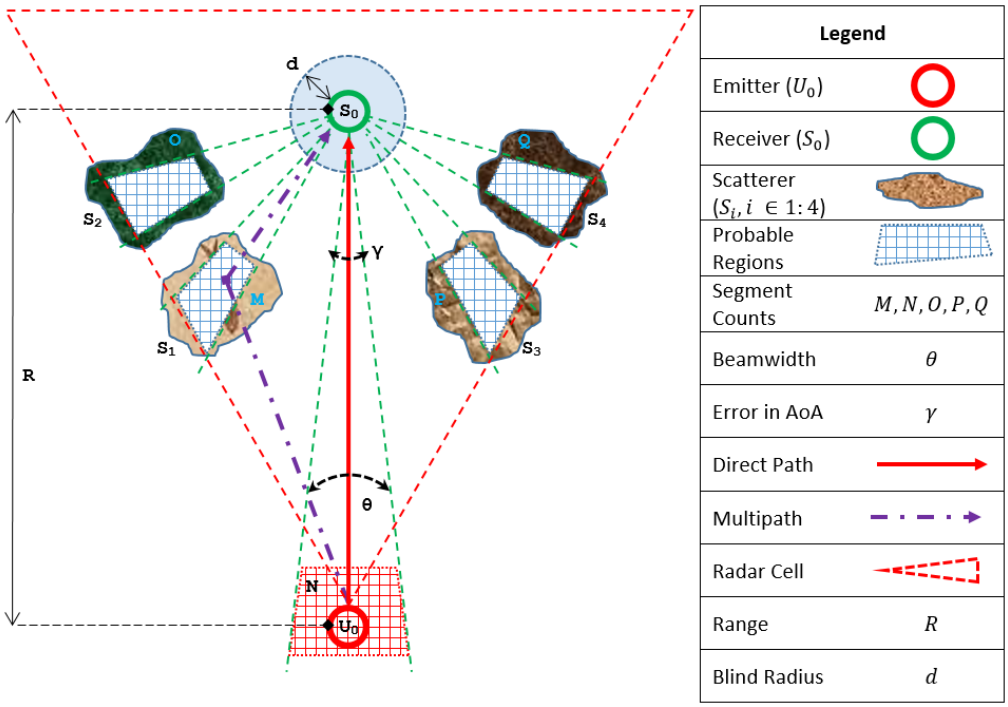

Figure 2.1: Simplified 2D problem space.

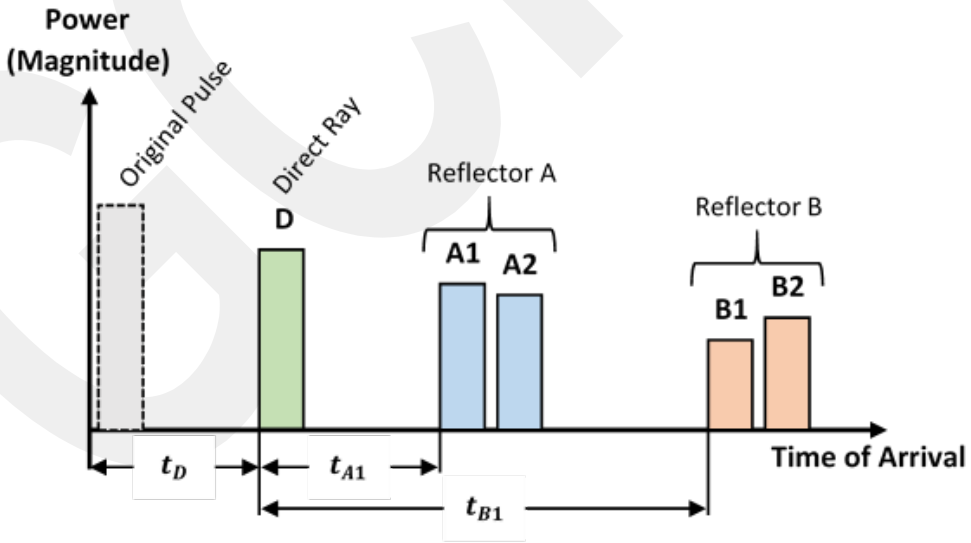

Figure 2.2: Intercept pulses in a multipath propagation environment.

the advantages of multipath effects in emitter localization. Essentially, the proposed method is based on the concept of utilizing multipath scatterers as artificial radar sensors to determine the emitter's position. To accomplish this, a recipe is employed, and its main steps are briefly described below. The algorithm's flowchart is depicted in Figure 2.3.

2.2.1 Phase I

The primary objective in this phase is to locate the scattering centers of multipath. In order to accomplish this, the ESM receiver provides the crucial AOA and TOA information for both the direct and multipath pulses. Consequently, it is imperative to determine the potential area of the multipath scattering centers.

During the initial step of this phase, the exterior bounds of the potential region for the multipath scattering centers are established. It is worth noting as one of the fundamental prerequisite that these must reside within the same radar cell. In this context, the radar cell size (r_c) represents the ground projection, as the problem is approached in a two-dimensional manner.

Moving on to the second step, the inner boundaries of the potential region for the multipath scattering centers are determined. This is achieved by fulfilling another requirement, which states that the direct path and multipath pulses should not overlap in terms of time scale. To prevent such overlap, the difference in TOA measurements (or TDOA) between the directly received and multipath pulses must exceed the pulse width of the radar emitter. Consequently, it becomes feasible to ascertain the minimum distance from the receiver to the inner boundary of the potential region for virtual sensors. However, it is important to emphasize that this distance can only be determined if the TDOA measurements are expressed in terms of range differences (RDs).

In the third phase, the width of the potential area containing multipath scattering centers is determined by the Angle of Arrival (AOA) of radar pulses, with an associated error margin (γ) as depicted in Figure 2.1. By incorporating the information obtained from all previous steps, it becomes feasible to accurately identify the probable region of multipath scattering centers on the rough surface.

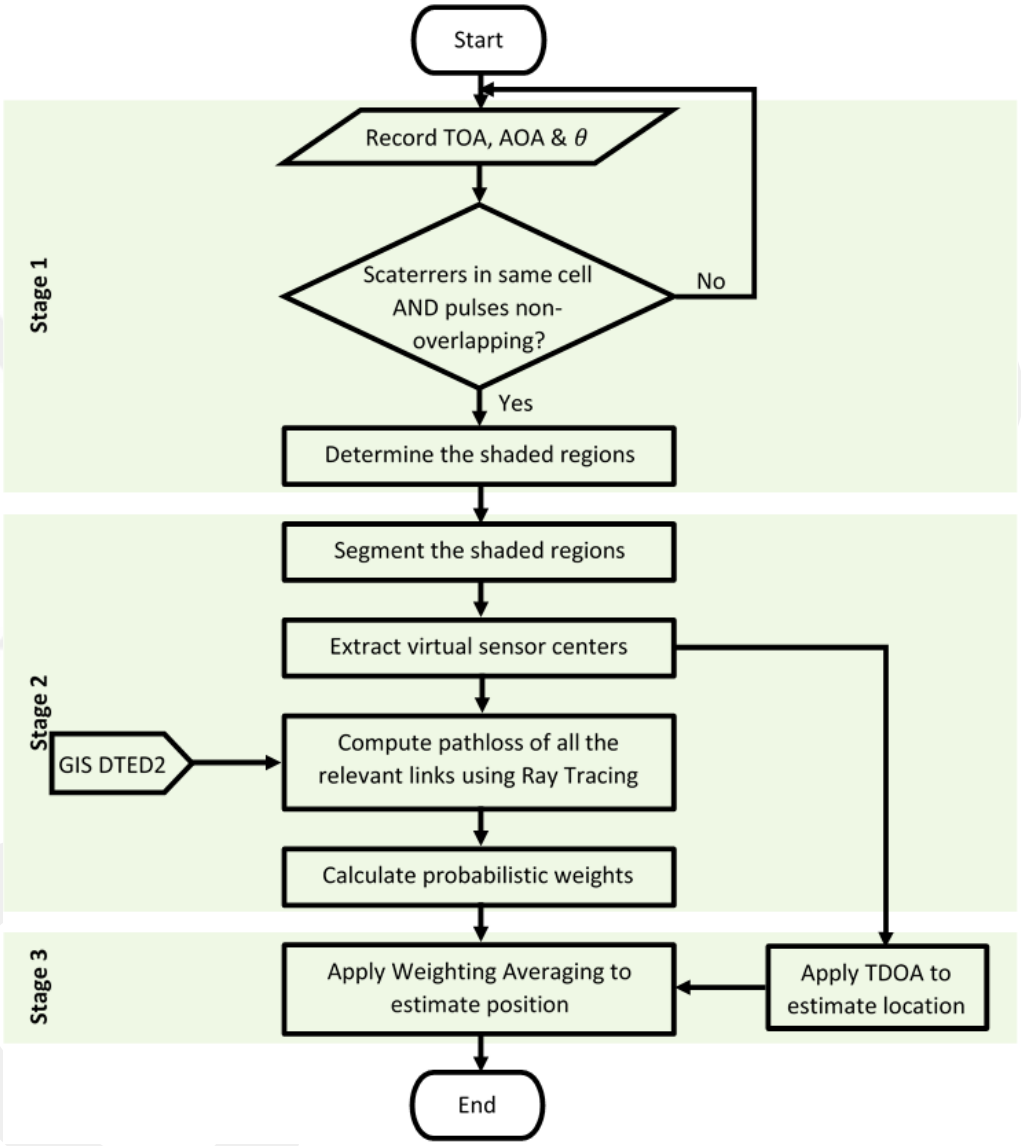

Figure 2.3: Flowchart of the proposed location estimation algorithm.

However, due to the irregular nature of these scattering centers in practical scenarios, the multipath waveforms undergo diffuse scattering. Consequently, the places pulses are scattered can be considered as a scattering center for multipath. Therefore, in the final step, a segmentation process is implemented, as illustrated in Figure 2.1, to divide the expected terrain of multipath scattering centers into distinct segments. Each of these segments can then be regarded as a multipath scattering center ($\mathbf{sc_{ij}}, i = 1, ..., N_j$ and $j = 1, ..., M$, where N_j represents the count of scattering centers in the j^{th} potential zone of artificial sensors, and M designates the number of virtual sensors).

Nevertheless, it is important to note that further analysis is necessary to establish the appropriate segments that are useful for the localization purposes. The assessment of the probability of the segments from which the multipath scattering arises enables the achievement of this objective. The subsequent phase entails a comprehensive examination of the precise particulars concerning this procedure.

2.2.2 Phase II

In this phase, the objective is to determine the probability, denoted as $p(\mathbf{sc}_{ij})$, of the scattering centers serving as a source of the multipath scattering through the utilization of a RT algorithm. It is crucial to highlight that the research outlined in [38] does not offer such an algorithm. Instead, it solely put forwards the theoretical framework of the procedure. Hence, this investigation endeavors to bridge this omission by presenting a performant RT algorithm. Subsequently, the theoretical foundation of the procedure is elucidated, followed by the explanation of how it is adapted to address the location estimation problem. Lastly, the calculation of the probability of the scattering centers is discussed.

2.2.2.1 Review of the Ray Tracing Algorithm

Computational electromagnetics for high frequency can be classified into two groups: field-based and current-based [91]. The current-based methods utilize Physical Optics to approximate short-wavelength phenomena. On the other hand, the field-based methods depend on Geometric Optics (GO). These field-based methods are particu-

larly suitable for radar frequencies commonly encountered in the current context of localization. In practice, the Ray Tracing (RT) methods are commonly employed for implementing these field-based methods [92]. The RT methods can be further divided into two: the image and the ray launching method. The image method relies on the concept of symmetry bearing on the short lines, determining whether the rays are obstructed by the segments or not. However, the image method suffers from computational complexity when dealing with myriad segments. It is worth mentioning that researcher have extensively published on various aspects of RT algorithms [93–95]. Therefore, for the wireless propagation prediction in the position estimation task addressed in this thesis, the ray launching method is considered a favorable option over the image method. Consequently, the ray launching method is employed in this thesis due to its inherent advantages.

The ray launching technique can be implemented in a series of three steps, namely ray initiation, ray tracing (RT), and ray interception [32]. During the ray initiation part, the beams are emitted with consistent angular spans. In the second step, the behavior of the rays is checked to decide if they encounter any obstacles. If an obstacle is encountered, the rays undergo specular reflection. The maximum number of reflections can be limited as per the task. If the first ray does not encounter any reflections, it is then passed on to the second ray. Once all the rays have been traced, they are converged at the intercept receiver.

Alternatively, in practical scenarios, the receiver can measure the directed, reflected, or diffracted wave. In such cases, the electric field of the LOS wave can be mathematically denoted as stated by Rizk et al. [96] as

$$E_{dir} = \frac{1}{r_0} \mathrm{e}^{-jkr_0}, \tag{2.1}$$

where the transmitter-receiver distance is r_0, and k is the wave number. Similarly, the electric field of the reflected waves can be formulated as

$$E_{ref} = R\frac{1}{r} \mathrm{e}^{-jkr}. \tag{2.2}$$

Referring to the Equation 2.2, r corresponds to the distance sum of the path traveling

from the transmitter to the incident point to the receiver antenna, whereas the reflection coefficient is denoted as R. Furthermore, the electric field of the diffracted waves can be mathematically presented according to the uniform theory of diffraction (UTD) model as [97]

$$E_{dif} = E_{in} \cdot D(\alpha) \cdot A(r) \cdot \mathrm{e}^{-jkr}, \tag{2.3}$$

where E_{in} is the inbound field, $A(r)$ is the spreading factor, and $D(\alpha)$ is the diffraction coefficient for diffraction angle α which in turn can be elaborated as [98]

$$D(\alpha) = -\frac{\mathrm{e}^{-j\pi/4}}{2\sqrt{2\pi}\cos(\alpha/2)} F[x]. \tag{2.4}$$

Here, α is the diffraction angle and $F[x]$ is the transition function given as [99]

$$F[x] = 2j\sqrt{x}\mathrm{e}^{-jx} \int_{\sqrt{x}}^{\infty} \mathrm{e}^{-ju^2}\,\mathrm{d}u, \tag{2.5}$$

where $x = 2kL\cos^2(\alpha/2)$ and L is the distance parameter given as

$$L = \frac{r_0 r_1}{r_0 + r_1}. \tag{2.6}$$

2.2.2.2 Adoption of the Ray Tracing Algorithm

In order to utilize the RT algorithm in the suggested position estimation task, it is essential that the scattering centers are visible to both the transmitter and the interceptor from an electromagnetic standpoint. Within this context, it is crucial to accurately define the probable region of the radar emitter. This is achieved by estimating the distance between the radar emitter and the receiver, taking into account the peak transmitting power of the radar emitter, the received power, and the measured erroneous AOA of the radar pulses (γ_i) by the receiver. Due to intrinsic limitations at either the source or the sink, the projected distance is expected to have some degree of error, which corresponds to the width of the region perpendicular to the direction towards the receiver.

Subsequently, as depicted in Figure 2.1, the region needs to be divided into segments, with each segment's center assumed as the nominal position of the radar emitter, denoted as $u_k = [x_k, y_k, z_k]$, where $k = 1, 2, ..., K$ and K represents the number of segments within the expected region of the radar emitter. This segmentation allows for the establishment of paths between the multipath centers and the nominal position of the radar emitter. To accomplish this, the center of each scattering center, denoted as $s_{ij}^0 = [x_{ij}^0, y_{ij}^0, z_{ij}^0]$, needs to be determined. This process enables the construction of links between the scattering centers and the receiver as well. Once the links have been established, the RT algorithm can be implemented to estimate the potential path loss (PL) caused by obstacles for the specific routes.

To adapt the RT algorithm, the initial step involves determining the specific area within a 3D map where the localization method is intended to be utilized. In this process, the algorithm relies on the utilization of the GIS elevation data. The DTED, a type of raster topographic data, provides essential quantitative data for systems that necessitate information on terrain elevation, slope, and surface characteristics. Selecting a higher level of DTED tiling scheme is of utmost importance when aiming to obtain accurate terrain data. Subsequently, a lateral terrain profile is derived from the three-dimensional map to establish the connections between the nominal positions of the radar emitter and the center of each scatterer, as well as between the center of each scatterer and the intercept receiver. Following this, the distance-height profile undergoes a redefinition through line segmentation to facilitate the application of the RT algorithm. A typical 2D terrain profile and line segmentation are illustrated in Figure 2.4.

Next, the transmitting and receiving points are positioned at the nominal positions of the radar emitter and the center of each scattering center, respectively, to establish the links between them. Similarly, for the links between the center of each scattering center and the receiver, the transmitting and receiving points are deployed at the center of each scattering center and the receiver, respectively. The RT algorithm is employed to determine the characteristics of all the direct, reflected, and diffracted waves on both links. Consequently, the electric field and the propagation map for a terrain profile can be accurately computed, taking into account the contributions of all these wave components. This comprehensive analysis also enables the estimation of the Path Loss (PL) for each link. To illustrate, Figure 2.5 presents a radio propagation map for a

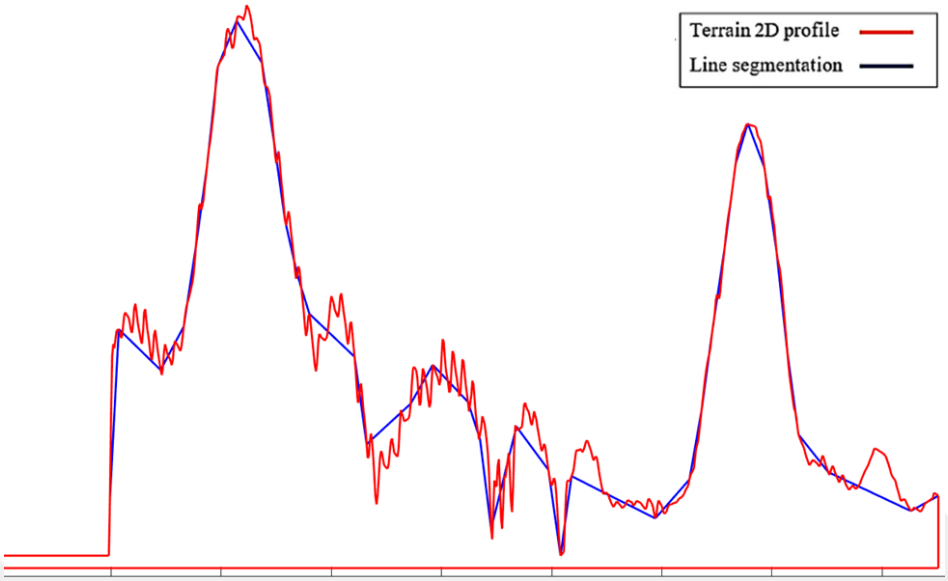

Figure 2.4: Line segmentation in RT algorithm.

two-dimensional terrain profile.

The propagation map, depicted in Figure 2.5, is derived from a combination of direct, diffracted, and reflected waves. Notably, the diffracted waves are particularly evident at the rear of the obstacle, where the electric fields experience a sharp reduction. It is important to highlight that the barriers are anticipated to coincide with the Fresnel zone, which is formed between the speculative positions of the source and the sink. Additionally, considering the insights articulated in Phase I regarding the identification of potential regions for multipath scattering centers, the obstructions are also anticipated to lie within the perpendicular plane that encompasses the speculative positions of the radar emitter and the receiver. Furthermore, it is crucial to acknowledge that the reflecting surface on the obstacle is assumed to be locally flat, resembling a line segment. Consequently, the phenomenon of specular reflection, also known as the Fresnel approximation, is anticipated. Moreover, due to the presence of edge- or wedge-shaped obstacles between the transmitter and the receiver, diffraction is also expected to occur. Consequently, both the reflected and diffracted waves originating from the obstructions can be measured at the receiver.

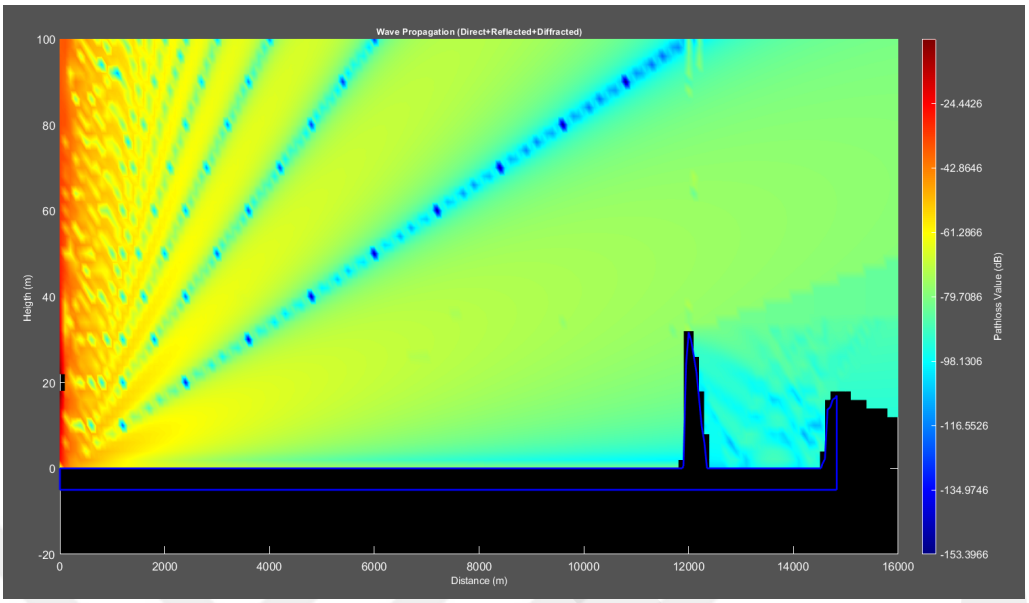

Figure 2.5: A typical propagation map.

2.2.2.3 Estimating Probabilities of the Scattering Centers

The determination of the probability of the scattering centers, denoted as $p(\mathbf{sc}_{ij})$, plays a crucial part in the practical deployment of the proposed localization method. In order to accurately calculate this probability, it is necessary to consider the total path loss (PL) or the total path gain (PG). This is due to the fact that different propagation mechanisms may exist for each segment in practice.

For this specific localization problem under consideration, the path loss for a specific channel comprises three components: the free-space path loss (PL_{FS}), the degradation in the received electric field caused by reflection (PL_R), and the loss resulting from diffraction (PL_D) as estimated by the RT tool. When there are no obstructions between the emitter and the ESM, the free-space path loss is utilized to calculate the strength of the electric field, as denoted in Equation (2.1).

Furthermore, the electric field of signals that undergoes one or more reflections can be determined using Equation (2.2). Additionally, diffraction occurs at edged surfaces, and the field strength of the diffracted waves can be calculated using Equation (2.3). In essence, the path loss for a fundamental link can be expressed as

$$PL[dB] = PL_{FS} + PL_R + PL_D. \tag{2.7}$$

It is anticipated that the receiver will receive more than one reflected or diffracted waves, as expected. The designed RT algorithm has the capability to identify and analyze rays undergoing reflections and diffraction up to six times. This includes a combination of reflection, diffraction, and additional reflections or diffractions. However, it is worth noting that the radar emitter localization problem typically requires only a few of these multiple reflections and diffractions to be considered.

It is crucial to acknowledge that the factors utilized in the calculation of the path loss (PL) can vary depending on the specific localization scenario. In certain cases, the diffracted signals may not be measurable due to the positioning of obstacles. In such instances, the path loss (PL) is simply composed of the free space path loss (PL_{FS}) and the reflection path loss (PL_R).

Clearly, it is necessary to estimate the path loss (PL) for all the scatterers within each potential area of virtual sensors. From a non-specific standpoint, the path gain value (PG) of the ith scattering center in the jth potential zone (PL_{ij}) can be found using the equation

$$PG_{ij} = \frac{1}{PL_{ij}}, \tag{2.8}$$

where,

$$PL_{ij} = PL_{\mathbf{u}_k \mathbf{sc}_{ij}} + PL_{\mathbf{sc}_{ij}\mathbf{s}_o^0}. \tag{2.9}$$

PL_{ij} is the total PL of the link between the nominal position of the radar emitter and the center of each scattering center ($PL_{\mathbf{u}_k \mathbf{sc}_{ij}}$) and the link between the center of each scattering center and the receiver ($PL_{\mathbf{sc}_{ij}\mathbf{s}_o^0}$) on the Equation 2.9.

Henceforth, $p(\mathbf{sc}_{ij})$, the probability of the scattering centers, can be expressed as

$$p(\mathbf{sc}_{ij}) = \frac{PG_{ij}}{\sum_{i=1}^{N_j} PG_{ij}}. \tag{2.10}$$

2.2.3 Phase III

In the third phase, the objective is to determine the location of the radar transmitter. The necessary approach to accomplish this objective are definitive. Initially, each scattering center's position is identified in Phase I is assumed as the apparent position of the virtual sensors. Consequently, the task of localizing a single sensor transforms into a task of localizing multiple sensors, which can be resolved using conventional techniques that utilize TDOA measurements. However, due to the presence of diffuse components caused by multipath scattering over uneven terrain, there is an expected level of uncertainty in the location of the scattering centers. In such cases, it becomes crucial to account for any inaccuracies in the positions of the virtual sensors. Therefore, it is essential to employ an effective source localization technique that incorporates TDOA measurements while considering sensor position errors. Based on the comparative results provided in [100], the improved-TSWLS technique introduced in [41] appears to be a suitable choice for implementation in the proposed localization method due to its efficiency in handling high sensor position errors. The subsequent section briefly outlines an adaptation of the improved-TSWLS technique to the proposed method. This is succeeded by a subsequent section that introduces the approach of weighted averaging employed to estimate the radar emitter.

2.2.3.1 The Improved-TSWLS Method

To comprehend the adaptation of the improved-TSWLS technique to the proposed method, we should consider the problem space as illustrated in Figure 2.1. In the figure, assume that there is only one virtual sensor in each of the probable regions of scattering centers, and there is only one nominal position of the radar emitter ($k = 1$), for the sake of simplicity. In this case, by considering 3D, there are M virtual sensors at locations $\mathbf{s}_j^o = [x_j^o, y_j^o, z_j^o]^T$, where $j = 0, 1, ..., M$ and the receiver $\mathbf{s}_0^o$, to localize the emitter, $\mathbf{u}^o$. In this scenario, the situation where $j = 0$ can be regarded

as the receiver's position, whereas the remaining values represent the positions of virtual sensors. In order to accommodate the uncertainty associated with the scattering centers' locations, it is necessary to take into account the presence of noise in the virtual sensor positions. Accordingly, a sensor position vector can be formulated as $\mathbf{s} = [\mathbf{s}_0^T, \mathbf{s}_1^T, ..., \mathbf{s}_M^T]^T = \mathbf{s}^o + \Delta\mathbf{s}$, where $\mathbf{s}^o = [\mathbf{s}_0^{oT}, \mathbf{s}_1^{oT}, ..., \mathbf{s}_M^{oT}]$ and $\Delta\mathbf{s}$ is the sensor position error vector, $\Delta\mathbf{s} = [\Delta\mathbf{s}_0^T, \Delta\mathbf{s}_1^T, ..., \Delta\mathbf{s}_M^T]^T$,which is assumed to be a zero-mean random variable and Gaussian distributed with the covariance matrix, $Q_s = E[\Delta\mathbf{s}\Delta\mathbf{s}^T]$. Since the position of $\mathbf{s}_0^o$ is unambiguous, the $\Delta\mathbf{s}_0$ should be comparable to zero.

To utilize the improved-TSWLS method, the reference sensor is designated as $\mathbf{s}_0^o$. Consequently, the TDOAs are represented as

$$\Delta t_{j+1,0} = (t_{j+1} - t_0), \tag{2.11}$$

where t_0 and $t_(j+1)$ are the TOA at the reference sensor and the jth sensor, respectively. Next, the time-differences can be transformed to the range-differences using

$$r_{j+1,0}^o = c\Delta t_{j+1,0} = c(t_{j+1} - t_0) = r_{j+1}^o - r_0^o, \tag{2.12}$$

where c is the speed of light, r_{j+1}^o is the Euclidean range between the source and the jth sensor, and r_0^o is the Euclidean range between the source and $\mathbf{s}_0^o$.

Furthermore, the transformed RD measurement vector can be mathematically represented as $\mathbf{r} = [r_{1,0}, r_{2,0}, ..., r_{M,0}]^T = \mathbf{r}^o + \Delta\mathbf{r}$ where $\mathbf{r}^o = [r_{1,0}^o, r_{2,0}^o, ..., r_{M,0}^o]^T$ and Δr is the measurement difference vector, $\Delta\mathbf{r} = [\Delta r_{2,0}, \Delta r_{3,0}, ..., \Delta r_{M,0}]$, which is assumed to be a zero-mean random variable and Gaussian distributed with the covariance matrix, $Q_t = E[\Delta\mathbf{r}\Delta\mathbf{r}^T]$.

The improved-TSWLS technique employs a two-stage approach to approximate the emitter location. During the first stage, a nonlinear measurement equation is linearized and solved by introducing nuisance parameters. To facilitate this process, an unknown vector, μ_1, is defined, which encompasses the initial estimates of the radar emitter and the distance between the emitter and the receiver. Subsequently, the weighted least-squares estimate of vector μ_1 is computed using

$$\mu_1 = (\mathbf{G}_1^T \mathbf{W}_1 \mathbf{G}_1)^{-1} \mathbf{G}_1^T \mathbf{W}_1 \mathbf{h}_1, \tag{2.13}$$

where

$$\mathbf{G}_1 = -2 \begin{bmatrix} (\mathbf{s}_1 - \mathbf{s}_0)^T & r_{1,0} \\ \vdots & \vdots \\ (\mathbf{s}_M - \mathbf{s}_0)^T & r_{M,0} \end{bmatrix}, \tag{2.14}$$

$$\mathbf{h}_1 = \begin{bmatrix} r_{1,0}^2 - \mathbf{s}_1^T \mathbf{s}_1 + \mathbf{s}_0^T \mathbf{s}_0 \\ \vdots \\ r_{M,0}^2 - \mathbf{s}_M^T \mathbf{s}_M + \mathbf{s}_0^T \mathbf{s}_0)] \end{bmatrix}, \tag{2.15}$$

and

$$\mathbf{W}_1 = (\mathbf{B}_1 \mathbf{Q}_t \mathbf{B}_1^T + \mathbf{D}_1 \mathbf{Q}_s \mathbf{D}_1^T)^{-1}, \tag{2.16}$$

where

$$\mathbf{B}_1 = 2\text{diag}[r_1^o, ..., r_M^o], \tag{2.17}$$

where diag[·] signifies the diagonal matrix.

Equation (2.13) encompasses the first three elements of μ_1, specifically $(\mu_1(1:3))$, which serve as an initial estimate for the radar emitter. Additionally, $\mu_1(4)$ denotes the final element of μ_1, representing the initial estimation of the distance between the source and the sink.

In the subsequent stage, the localization error of the first stage is assessed and subsequently subtracted from the output of the initial stage. To facilitate this process, the second stage commences by updating Equation (2.13) as

$$\mu_2 = (\mathbf{G}_2^T \mathbf{W}_2 \mathbf{G}_2)^{-1} \mathbf{G}_2^T \mathbf{W}_2 \mathbf{h}_2, \tag{2.18}$$

where

$$\mathbf{G}_2 = \begin{bmatrix} \mathbf{I}_{(3,3)} \\ -\mu_1(1:3)-\mathbf{s}_0 \big/ \|(\mu_1(1:3)-\mathbf{s}_0)\| \end{bmatrix}, \tag{2.19}$$

$$\mathbf{h}_2 = \begin{bmatrix} \mathbf{0}_{(3,1)} \\ \mu_1(4) - \|(\mu_1(1:3) - \mathbf{s}_0)\| \end{bmatrix}, \tag{2.20}$$

and

$$\mathbf{W}_2 = \mathbf{B}_2(\mathbf{G}_1^T\mathbf{W}_1\mathbf{G}_1)^{-1}\,\mathbf{B}_2^T, \tag{2.21}$$

where

$$\mathbf{B}_2 = \begin{bmatrix} -\mathbf{I}_{(3,3)} & \mathbf{0}_{(3,1)} \\ \mathbf{0}_{(3,1)}^T & 1 \end{bmatrix}. \tag{2.22}$$

In Equation (2.22), $\mathbf{I}_{(3,3)}$ corresponds to an identity matrix of dimensions 3×3 and $\mathbf{0}_{(3,1)}$ corresponds to a 3×1 zero vector. Thus, the estimated nominal location of the radar emitter can be found using

$$\hat{\mathbf{u}} = \mu_1(1:3) - \mu_2. \tag{2.23}$$

2.2.3.2 The Weighted Averaging Method

In practical scenarios, it is common to have multiple virtual sensors distributed across various potential zones of scattering centers. Additionally, there may exist multiple speculative positions for the transmitter within the expected region. As a result, the localization problem becomes complex and necessitates further approaches for resolution. To address this, the first step involves the creation of virtual sensor groups by taking into account all possible groupings of virtual sensors chosen from the M probable sensor zones. These groups are then utilized in conjunction with the improved-TSWLS technique. Consequently, scattering center groups are also formed. This enables the calculation of likelihoods for the scattering center groups ($\mathbf{p}_t, t = 1, 2, ..., T$, where T signifies the virtual sensor group counts). The reliability of a series system

is taken into account during this calculation, as described in Trivedi's work [101] on probability. Subsequently, for each scattering center group, the speculative position of the radar emitter is estimated using the improved-TSWLS method as

$$\hat{\mathbf{u}}_{k,t} = \begin{bmatrix} \hat{\mathbf{u}}_{k,1} & \hat{\mathbf{u}}_{k,2} & ... & \hat{\mathbf{u}}_{k,T} \end{bmatrix} \tag{2.24}$$

for $k = 1, 2, ..., K$ where K is the count of segments of the tentative area of the transmitter source.

Hence, in order to determine the emitter's location, the weighted averaging technique is employed as

$$\overline{\mathbf{u}}_k = \sum_{t=1}^{T} \mathbf{p}_t \times \hat{\mathbf{u}}_{k,t}, \tag{2.25}$$

and, the final estimate of the emitter position ($\overline{\overline{\mathbf{u}}}$) can be expressed as the mean of all the position estimations as

$$\overline{\overline{\mathbf{u}}} = \frac{1}{K} \sum_{k=1}^{K} \overline{\mathbf{u}}_k. \tag{2.26}$$

In conclusion, it is important to highlight that the localization method proposed in this thesis deviates from conventional approaches that rely on multiple sensors or wireless sensor networks. Instead, the author utilizes virtual sensors derived from multipath scattering centers, along with a single antenna that captures both direct and multipath waves. These signals are then analyzed to estimate the emitter's position. Consequently, unlike traditional methods, the adaptation of the introduced technique necessitates the establishment of communication links between the sensors or between the emitter and sensors for the successful execution of the RT algorithm, as previously discussed.

2.3 Problem Statement

There are some important concerns with the implementation of the localization algorithm presented in the previous subsection. These can be listed as

1. Sensor Placement & Orientation
2. Sensor Geometry
3. Combinatorial Complexity

2.3.1 Sensor Placement & Orientation

TDOA-based location estimation solutions extensively use sensor characteristics and are sensitive to perturbations. The accuracy farther deteriorates in the cases of passive emitter localization due to factors like sensor position noise and measurement errors. It is typically unpractical to use all the sensors in localization as the system requirements would void the system usability. Therefore, some form of sensor selection needs to be in place to exclude the nonviable sensors. Furthermore, four sensors are necessary in TDOA-based localization systems in 3D like this thesis aims to. Numerous methods have been suggested in scholarly works to rectify this [102–104]. Literature uncovers various orientation of sensors like straight, trapezoidal, parallelogram, rectangle, lozenge, inverted triangle, square, and Y-shape. Nevertheless, we must also investigate a proper orientation scheme for the passive multipath exploiting emitter localization method proposed here. To do so, three simple but imperative sensor orientations in realistic scenarios will be probed.

2.3.2 Sensor Geometry

Another important aspect that may highly affect the localization accuracy is the localization geometry. This is closely related to the sensor position and orientation briefly discussed earlier. Localization accuracy is expected to drop in the case that the radar has a narrow beamwidth, where the virtual sensor positions could be close to each other and the radar emitter is distant from the sensor layout. Generally, the geometrical

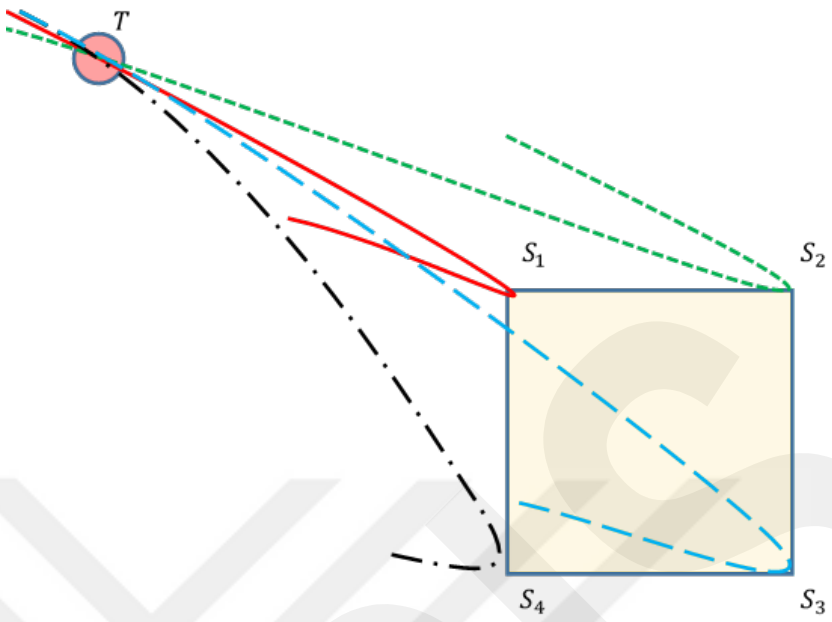

Figure 2.6: Bad GDOP leading to near-parallel hyperbolic lines.

effect on location estimation can be described by the GDOP [105, 106]. Particularly, a large GDOP indicates poor localization accuracy. This is because, when the target is at a considerable distance from the baselines between the sensors, the hyperbolic lines of positions (LOPs) in TDOA-based localization are nearly parallel in this region, and noise or small measurement errors can cause considerable errors in computing the geolocation. Figure 2.6 illustrates one such sensor orientation where hyperbolic lines of ranges are near-parallel at the target. In other words, the TDOA accuracy is affected by the orientation of the scatterer centers or GDOP.

For the problem considered in this thesis, the GDOP is determined as given in the following

$$GDOP = \sqrt{tr(H^T H)^{-1}}, \tag{2.27}$$

where the operator $tr(\cdot)$ denotes the matrix trace and the geometry matrix H consists of the pseudorange measurement residual equations of the virtual sensors. For a given virtual sensors selected from M scatterer regions, it can be expressed by

$$H = \begin{bmatrix} \frac{x_1^o - x_0^o}{R_1} & \frac{y_1^o - y_0^o}{R_1} & \frac{z_1^o - z_0^o}{R_1} \\ \frac{x_2^o - x_0^o}{R_2} & \frac{y_2^o - y_0^o}{R_2} & \frac{z_2^o - z_0^o}{R_2} \\ \vdots & \vdots & \vdots \\ \frac{x_M^o - x_0^o}{R_M} & \frac{y_M^o - y_0^o}{R_M} & \frac{z_M^o - z_0^o}{R_M} \end{bmatrix}, \tag{2.28}$$

where R_M is the Euclidean distance in 3D between the M^{th} virtual sensor and the receiver.

Therefore, since the problem of radar emitter localization considered in this research work is scenario-dependent, it can be inferred that the GDOP could be used as an important criterion for further enhancements of the localization efficiency.

2.3.3 Combinatorial Complexity

Alternatively, for the cases the radar source exhibits a wide beam angle, this approach can offer superior accuracy in localizing targets. However, a wider beamwidth leads to larger scatterer regions. In this case, there might be many virtual sensor and scattering center groups to be successively used in the localization algorithm. More specifically, assuming each of M scatterer regions consists of N segments (scattering centers) would lead to the use of a combination of N^M, which corresponds to a computational complexity of $O(N^M)$. This then results in an increase in computational costs and memory needs. Thus, for large-scale operational scenarios, memory overflow might occur in the adaptation of the localization algorithm. Hence, due to the significant increase in resource requirements and computation time, the applicability of the localization method becomes questionable. Hence, it is apparent that additional investigation is required to minimize the computational expenses associated with the localization method through the incorporation of supplementary approaches and strategies. Subsequently, the subsequent section introduces a data-driven approach that can effectively diminish the computational cost of the localization method.

CHAPTER 3

EXPERIMENTS & RESULTS

In order to evaluate the practicality of the emitter localization using multipath signals in a single receiver setup, the author pursues a two-fold experimentation. Firstly, the section 3.1 uses simulation to assess the feasibility of the proposed approach within the EW context. Here, virtual sensor placements or positions in relation to the stationary intercept receiver are investigated. As a result, the adverse affect of GDOP on the localization accuracy is properly researched. This analysis alone is not sufficient to develop a deployable localization system due to the immense amount of computational resource requirements discussed earlier chapter. As a remedy, a data-driven modern approach is suggested in section 3.2 which is well-suited to the passive localization being analyzed. Three different ML techniques are explored and analyzed to compare the performance gains in terms of both the estimation error and execution time.

3.1 Sensor Placement & Geometry

3.1.1 Simulation

This section provides the outcomes of simulations carried out to assess the practicality and accuracy of the localization method in real-life test cases. To construct the scenarios, a specific portion of the Mediterranean Sea is selected from the GIS map, as depicted in Figure 3.1.

The DTED data was utilized to generate a GIS map for a specific region in the Aegean Sea (3.2). Subsequently, three distinct simulation experiments were conducted, each

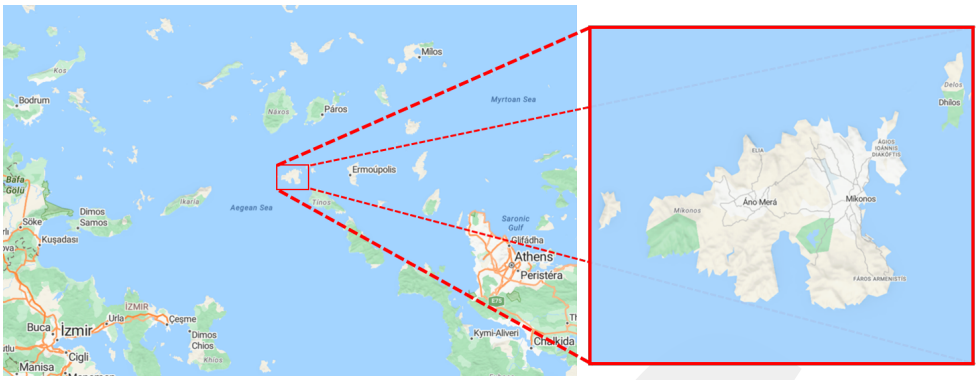

Figure 3.1: The Aegean Sea region, and The Mykonos Islands

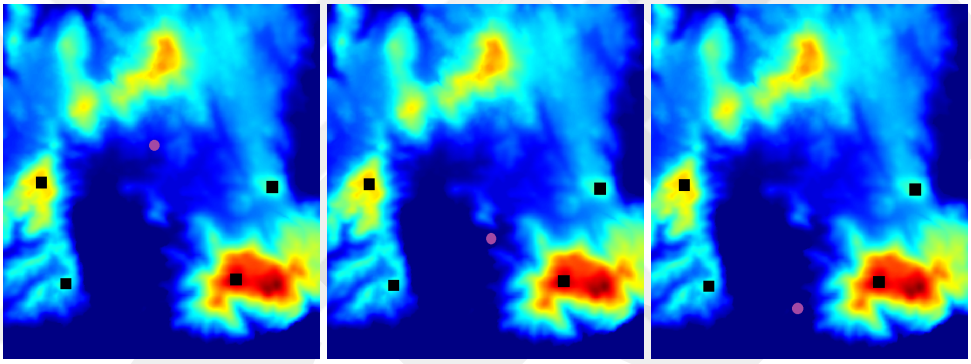

(a) (b) (c)

Figure 3.2: Receiver placements (a) back, (b) center, and (c) front in relation to sensors.

involving different scenarios by altering the position of the receiver relative to the scatterers. In the first experiment, the receiver was positioned behind the virtual sensors, whereas in the second experiment, it was placed at the near-center of the sensors. Finally, in the last experiment, the receiver was placed at the front relative to the virtual sensors. To illustrate, Figure 3.2 depicts the stationing of the ESM receiver (circle), and scatterers (rectangle) for a radar beam angle that remains fixed.

During each experiment, the radar specifications were configured to replicate the localization orientation depicted in Figure 2.1. The primary criterion of interest in this context is the pulse width (τ) of the radar emitter, which was set to 1μs for all the conducted experiments. Another significant parameter is the beamwidth (θ) of the transmitter, which was envisioned to be 10°, 15°, and 20°. Moreover, it was assumed that $\mathbf{s}_0^o$ has the ability to estimate five different angles of arrival (AOA)

information of radar pulses with a measurement uncertainty of ($\gamma = 3°$). In this particular configuration, it was postulated that four potential regions of scattering centers ($M = 4$) could be obtained after setting aside the direct pulse's AOA. In each simulation, the multipath pulses' AOA was set based on the randomly selected positions of the scatterers residing in the radar view. Only the incident bearing of the direct pulse remained constant in each case ($\gamma_0 = 90°$).

The segmentation process involved the identification of probable regions containing scattering centers for each setup. To accomplish this, a specific DTED tiling scheme was employed, with each segment measuring $25 \times 25 m^2$. It is important to highlight that the use of smaller-sized segments leads to a more accurate localization method. This increased accuracy can be attributed to the reduced noise in virtual sensor locations that arises as smaller segments are utilized in the segmentation process. Consequently, the noise power of the virtual sensor positions was calculated to be 6 dB using the fundamental empirical rule of normal distribution, which was then applied in the TDOA approach. Furthermore, the receiver-transmitter range (r_0^o) was set at 30, 40, and 50 km, respectively. It is worth noting that the range was capped at 50 km to prevent signal fading owing to the curvature of the planet. Additionally, the potential location of the emitter source was divided into nine segments ($K = 9$), with each segment's center serving as the speculative position of the radar emitter ($\mathbf{u}_k$, $k = 1, 2, ..., K$.

The RT method, as described in Section 2.2.2.2, was utilized to estimate the likelihood of scattering centers for each scenario. The localization algorithm then selected the top-five scattering centers with the highest likelihood from each expected zone of the artificial sensors. It is important to mention that both the radar emitter and receiver were assumed to be deployed on naval ships, with an antenna height of 60m. Furthermore, the geographic altitudes of the virtual sensors spread between 300m and 450m based on the geolocation of the scatterers on the digital three-dimensional map.

Subsequently, simulations were conducted to assess the performance of the localization method. The accuracy of the localization algorithm was evaluated by obtaining the mean square error (MSE) of the radar emitter location estimate using

$$\mathrm{MSE}(\overline{\overline{\mathbf{u}}}) = \frac{1}{L}\sum_{v=1}^{L} \|\overline{\overline{\mathbf{u}}}_v - \mathbf{u}^o\|^2. \tag{3.1}$$

In the given thesis, the Equation 3.1 is utilized to estimate the position of $\mathbf{u}^o$ in the vth ensemble run, denoted as $\overline{\overline{\mathbf{u}}}_v$ [41, 107]. The number of ensemble runs is denoted as L. The authors obtained the mean squared errors (MSEs) of the location estimates through 10^3 ensemble runs in their simulations. These MSEs were then contrasted with the MSE estimates of the improved-TSWLS approach to assess the reliability of the introduced technique. Nonetheless, the direct application of the improved-TSWLS method to tackle the localization problem proved to be unfeasible. As a result, a relaxation was implemented in the localization geometry for each individual scenario. This relaxation involved designating the center of each potential region encompassing the scattering centers as a sensor position, which would subsequently be employed in the improved-TSWLS method.

Figure 3.3 illustrates the estimation precision of the improved-TSWLS and the introduced localization approach in the first experiment. The findings indicate that the proposed method may not be accurate when the ESM is positioned at the rear of the sensors. Additionally, the improved-TSWLS method generally yields inaccurate outcomes. However, a significant discovery pertaining to the position estimation quality is that the accuracy tends to improve as the beam angle θ increases. Consequently, if the ESM is situated at the hind side of the sensors, the suggested approach is likely to offer a relatively precise localization, particularly if the targeted source operates in a broader beam angle.

Figure 3.4 depicts the precision of the improved-TSWLS and the suggested technique for experiment two. The outcomes attained from the improved-TSWLS approach that a conventional TDOA-based relying on WSNs may not be effective for the given position estimation application. Then again, in contrast to the prior simulation, the proposed method demonstrates noticeable improvements in both efficiency and robustness, as evident from the results. Regardless of the distance and beam angle, the introduced approach consistently delivers precise outcomes, with the highest approximation uncertainty reaching around 50 dB, corresponding to a distance of around 320 m.

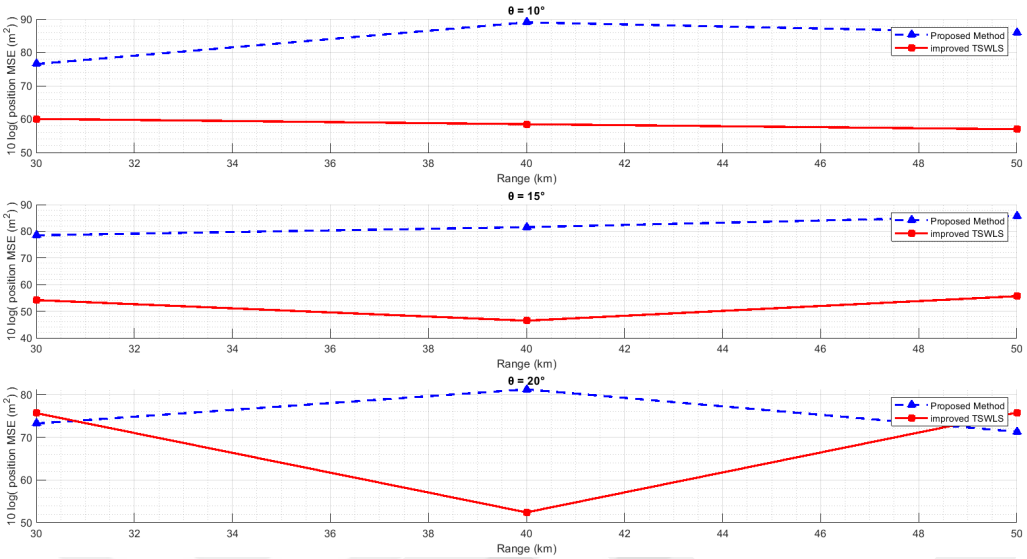

Figure 3.3: Positional error comparison for 3.2(a) setup.

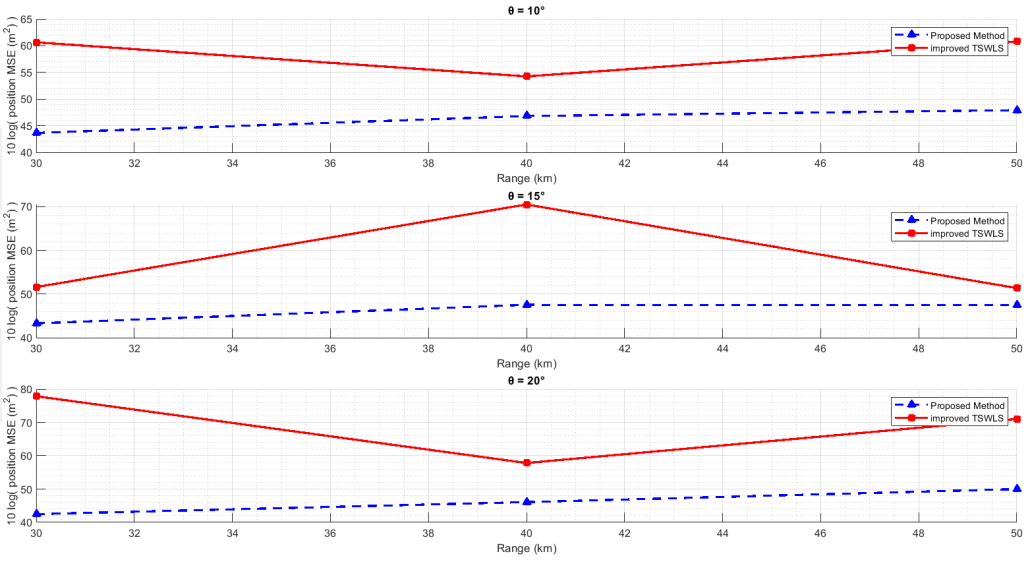

Figure 3.4: Positional error comparison for 3.2(b) setup.

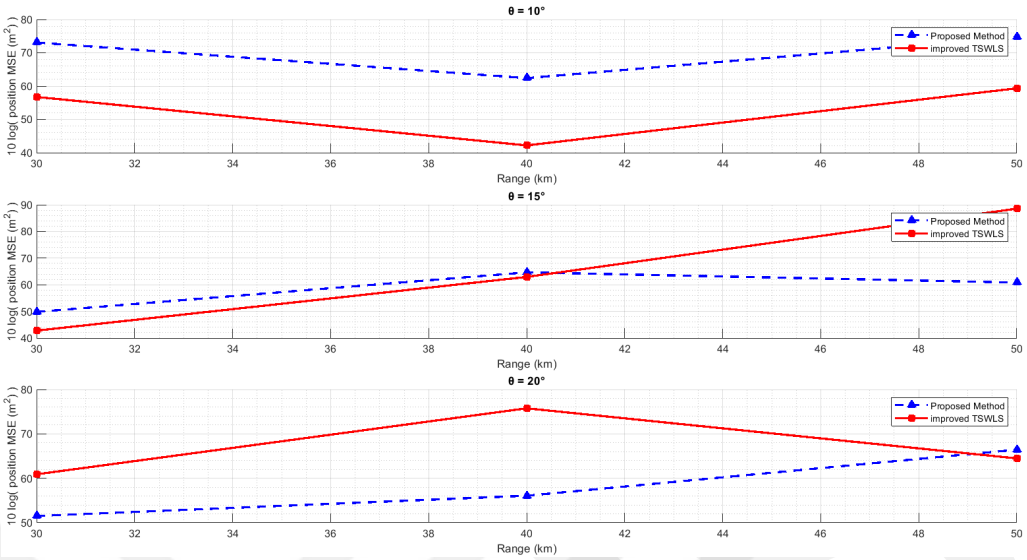

Figure 3.5: Positional error comparison for 3.2(c) setup.

In Figure 3.5 the localization quality of the improved-TSWLS and the suggested approach in the last experiment is presented. The figure reveals that the results exhibit inconsistency when $\theta \leq 10°$. In essence, akin to the outcomes of the preceding experiments, the precision of the suggested approach exhibits an inclination to enhance with the augmentation of the parameter θ. Consequently, the suggested approach is anticipated to be highly effective in locating the radar emitter, particularly at close proximity when the ESM is positioned before the sensors.

3.1.2 Discussions

The simulations conducted have confirmed that the suggested position estimation approach is largely feasible within the EW context, with the exception of certain specific localization scenarios. It should be noted that while the overall accuracy of the method in realistic scenarios is satisfactory, its performance is contingent upon the placement of the virtual sensors. This dependence arises from the actuality that TDOA-based techniques are significantly influenced by the geometric arrangement of the sensors. In particular, when faced with unfavorable geometry, the accuracy of the localization method is expected to decline. The underlying cause for this degradation can be ascribed to instances of high GDOP, which serves as a standard for assessing the

geometric impact of sensor configurations on localization accuracy [105]. In essence, a larger GDOP value indicates a poorer localization performance of the system. The simulation results presented in the previous section clearly demonstrate the GDOP effect within this context. The results clearly demonstrate that the lowest level of accuracy is attained when the ESM is located in front of scatterers, whereas the highest level of accuracy is reached when the ESM is positioned at the center of scatterers. Therefore, a lower GDOP value is associated with a better localization accuracy, which is consistent with previous studies that have examined GDOP values for different geometries [102, 108]. Additionally, the distance between the emitter and the receiver also plays a crucial role in adversely affecting the GDOP, as observed in the simulation results. Specifically, it is evident from each experiment that the suggested approach offers improved position estimation precision in short-distanced applications.

Moreover, the precision of the suggested approach in determining the location may be compromised when the radar emitter being targeted possesses a tight beam angle ($\theta \leq 10^{\circ}$). This limitation arises from the fact that when the transmitter has a narrow beam angle, the probable regions of the multipath scattering centers become narrower as well. Consequently, the virtual sensor positions are anticipated to be in close proximity to each other. As a result, the location geometry suffers, leading to a phenomenon known as large GDOP. Therefore, in order to enhance the accuracy of localization systems, it becomes imperative to establish an optimal geometric arrangement between the transmitter and virtual sensors. In this regard, the GDOP can serve as a metric for choosing suitable scatterer center combinations. By utilizing virtual sensor groups that yield the minimum GDOP, the objective of achieving higher accuracy can be realized.

The achieved outcomes show promise; however, they do not meet the requirements for a practical localization system due to the unresolved problem of computational complexity. Henceforth, the center orientation will be employed to augment the accuracy of passive localization.

3.2 Data-Driven Approach

To address the localization problem investigated in this thesis, a cost-effective alternative method is suggested, which involves the integration of machine learning models and measurements. This section provides a comprehensive description of the proposed approach.

Today, continuous advancements in ML techniques have enabled many people to solve complex issues in various fields. Particularly, specialized ML techniques are capable of outperforming traditional systems by learning the intricate hidden traits of the system. Essentially, ML leverages real-world data to educate an ML model in order to comprehend the intricate connections between the input data (features) and the output values (labels).

There exist three fundamental categories of machine learning, namely supervised learning, unsupervised learning, and reinforcement learning. Supervised learning finds its ideal application in datasets with clear labels, where the algorithm's training process is guided by well-defined examples. On the other hand, the realm of unsupervised learning opens up to the exploration of unlabeled data, empowering algorithms to discern hidden patterns and structures without the constraints of predefined categories. Reinforcement learning, on the other hand, installs agents in a dynamic environment to maximize the cumulative reward. Based on these ML types, various methods were proposed for outdoor emitter localization in the literature [13, 109–113]. However, the supervised learning is very popular for emitter localization tasks. This is because, with the regression analysis that falls under supervised ML, it becomes easy to predict the location of the emitter by creating a relationship between a set of dependent (coordinates) and independent variables (fingerprints) [114]. This suggests that a supervised ML-based approach can be an efficient means to facilitate the radar emitter localization considered in this thesis work.

The framework of the proposed approach is shown in Figure 3.6. The idea behind the approach is that the location of the radar emitter can be estimated by using a supervised ML model that was trained with a dataset containing the useful features of the data obtained from the problem geometry. In other words, the computational cost of the

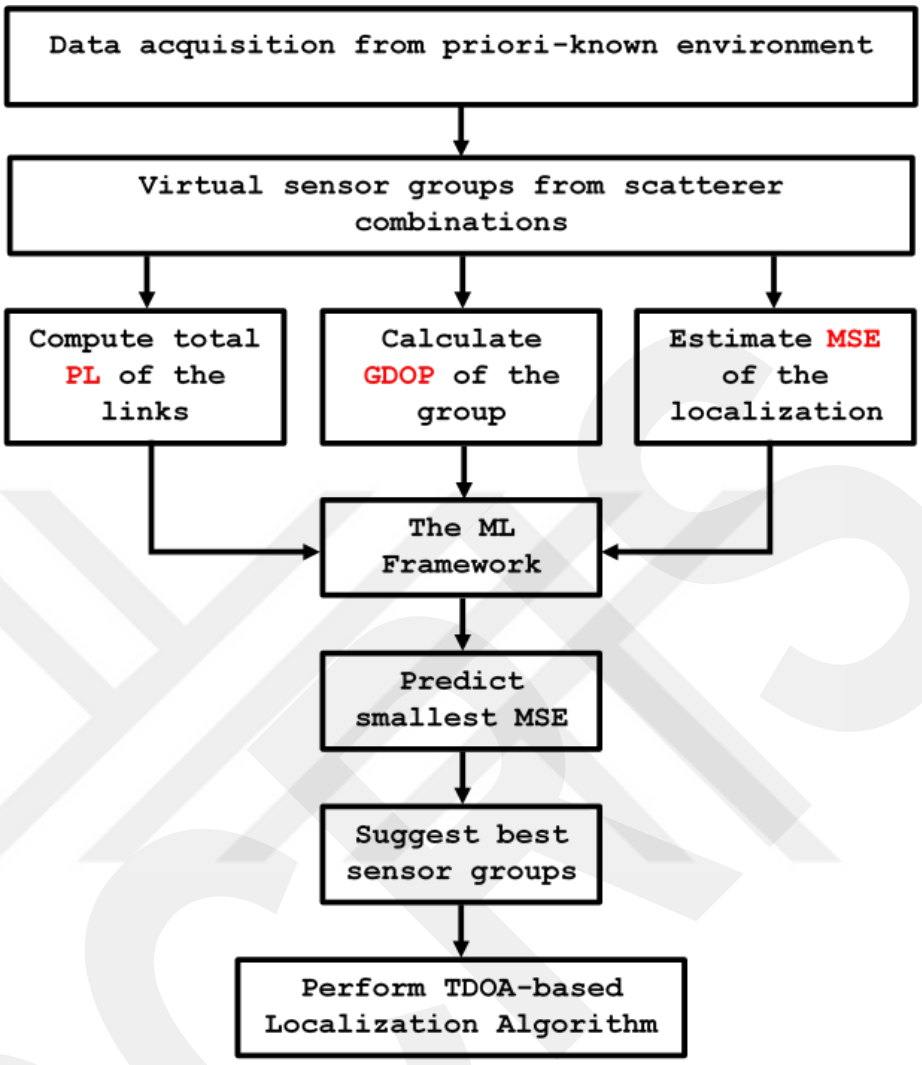

Figure 3.6: The framework of the proposed approach.

method presented in [39] can be reduced by adapting a data-driven approach, provided that the operational environment is priori-known. However, in order to construct such an approach, it is necessary to select the features carefully so that they hold meaningful information about the operational environment. Here, one of the features is the PL values of the emitter-scattering center-receiver links that can be calculated by the RT algorithm since the channel characteristics are known in general. It should be noted that the total path loss consisting of each of the scatterer regions needs to be grouped separately. That is, M path loss values can be recorded for each virtual sensor combination accordingly.

On the other hand, the GDOP-assisted outdoor localization methods have seen quite an interest in the past few years [115, 116]. Hence, to enhance the stability and performance of the approach, the GDOP value can be selected as a second feature. However, to calculate the GDOP value by (2.27), each virtual sensor group needs to be considered. Each virtual sensor combination then forms exactly one GDOP value.

Therefore, for a virtual sensor (scattering center) group, the PL values of the emitter-scattering center-receiver links, and the calculated GDOP value are inputted into the ML framework that attempts to predict the MSE of the radar emitter location estimate as the label. In addition to these, for the same virtual sensor groups, the MSEs of the location estimate obtained by the method presented in Section 2.2 are also fed into the ML framework. Here, the MSE of the location estimate can be obtained from Equation (3.1). Thus, it is expected to achieve a virtual sensor group that has the potential to provide an optimal location estimate in terms of low MSE. The achieved sensor group can then be used in one of the accurate localization algorithms based on TDOA measurements proposed in the literature to estimate the position of the radar emission source.

Needless to say, ML methods often undergo testing followed by rigorous training on gigantic quantities of data that are descriptive enough but not redundant to contaminate for the targeted system to properly construct a working model, which in turn enables performance analysis of the trained and tested model. Thus, a huge data sample collected from the operational environment is strictly required to implement the proposed approach properly.

3.2.1 Experiments

Experiments were conducted to evaluate the effectiveness of the ML-based approach in terms of both accuracy and computational efficiency in realistic scenarios. In this section, firstly, the method used for data acquisition is explained. This is followed by a description of the ML models used in the experiments. Then, the training details of the ML models are given. Lastly, the results achieved from the experiments are discussed.

3.2.1.1 Data Acquisition

Before conducting the experiments, it was necessary to create a dataset consisting of a huge amount of data collected from the given context of the problem space. Hence, the terrain profiles of a particular region determined over the Aegean Sea needed to be varied. Therefore, virtual terrain profiles were generated to be used in data acquisition.

In the literature, rendering realistic terrain has been used to provide important information to control or enhance instrument-guided systems in various domains, such as air navigation [117], geography [118], and vegetation [119]. In this thesis, the author was interested in producing terrain that appears to have been generated by real-world processes. In fact, the main motivation was to focus on terrain generation from real-world examples. In this context, in order to create realistic scenarios, a specific region of the Aegean Sea was selected from the 3D map, and then, its GIS map was generated. A top view of the region selected from the Aegean Sea and GIS three-dimensional map is shown in Figure 3.7(a) and Figure 3.7(b), respectively. The terrain profile of the region was then reproduced by generating pseudo-realistic terrain models. A sample of the generated pseudo-realistic terrain models is shown in Figure 3.8.

In order to generate a pseudo-realistic terrain model, it is important to model the landform features, specifically the mountains and the hills, which in fact contribute to the reflection, refraction, and diffraction of a traveling electromagnetic signal. Consider a problem space in a 3D rectangular grid of size $m \times n$ defined by $[X, Y] = \{X \in \mathbb{R} \mid X_L \leq X \leq X_H; Y \in \mathbb{R} \mid Y_L \leq Y \leq Y_H\}^{(m \times n)}$, such that X and Y are uniformly sampled and have exactly m and n number of unique but not necessarily disjoint samples, respectively. In other words, $[X, Y]$ denotes the region of interest. Then, any naturally or artificially occurring terrain can be modeled by a sufficient number of landform features, $N \in \mathbb{N}$, each of which has a height h above the sea or plain surface, a width w, and is located at the coordinate (x, y). Given the inherent randomness of nature, the height, width, and feature location can be parametrized as $H_N \sim U[H_L, H_H]$, $W_N \sim U[W_L, W_H]$, X_N $U[X_L, X_H]$, and $Y_N \sim U[Y_L, Y_H]$, where H_N, W_N, X_N, and Y_N are the height, width, and gridded positions, are uniformly distributed in the closed range of $[H_L, H_H]$, $[W_L, W_H]$, $[X_L, X_H]$, and $[Y_L, Y_H]$, respectively. Here, the subscript N denotes the feature size, and the lower and higher bounds of the ranges are signified

(a)

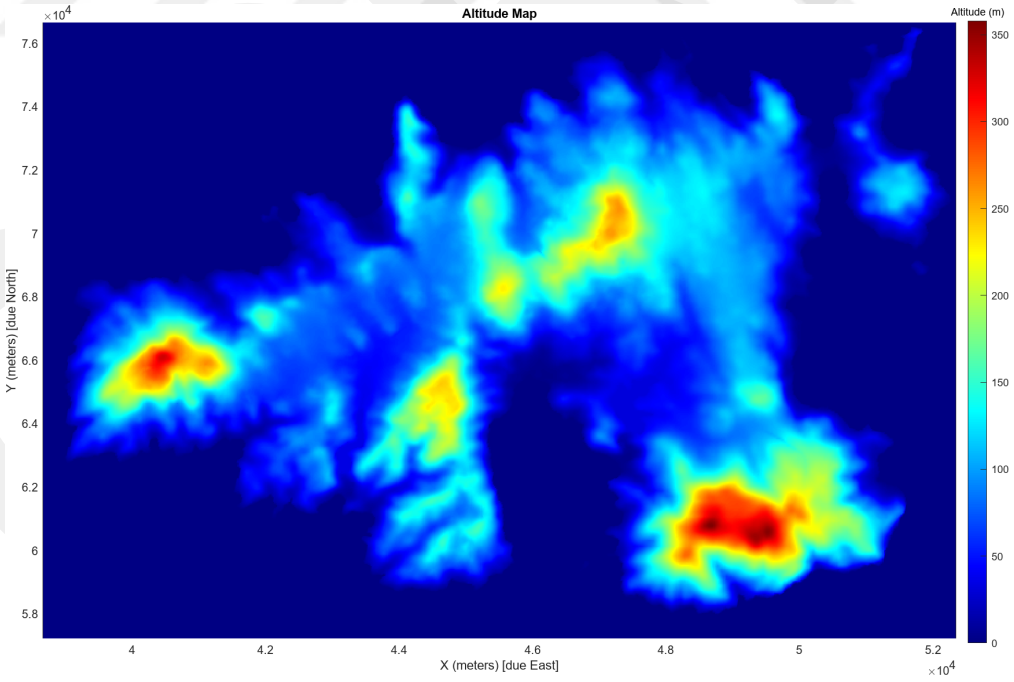

(b)

Figure 3.7: (a) A top view of the Mykonos Islands, and (b) the respective GIS height map.

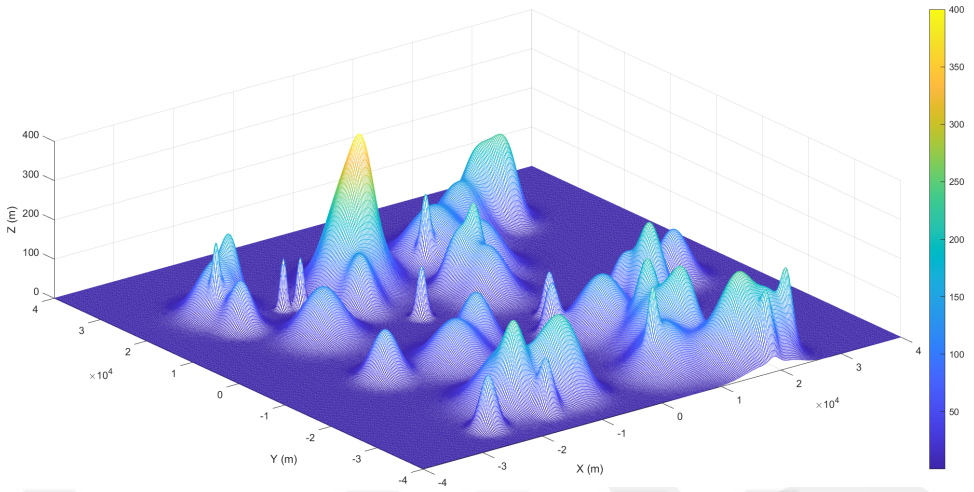

Figure 3.8: A sample of the generated pseudo-realistic terrain models.

by L and H. Consequently, the elevation profile, T, can be expressed as the product of the height function $G(h, w)$ and the modified Gaussian function. Therefore, the landform features (LF) can be mathematically modeled as

$$\mathrm{LF} = \sum_{\substack{h \in H_N \\ w \in W_N \\ (x,y) \in (X_N, Y_N)}} G(h, w)\, e^{-\frac{1}{W}[(X-x)^2 - (Y-y)^2]}. \tag{3.2}$$

The next step is to employ the problem space to generate pseudo-realistic terrain models as depicted in Figure 3.8. It is crucial to note that the placements of the landform features on the simulated map need to be parametrized, including their locations, and AOAs with respect to the intercept receiver, height, and width. Furthermore, it is necessary to obtain LOS paths between the emitter and the elevation profile on the simulated terrain, such that at least M virtual sensors need to be attainable. Thus, a pseudo-realistic terrain model consisting of M number of scatterer regions can be formulated by superimposing the terrain information as

$$S = \sum_{s=1}^{M} \mathrm{LF}_s. \tag{3.3}$$

Before generating the data, various simulation scenarios were created. In each of the scenarios, the ESM intercept was fixed at the center of the virtual sensor groups on

the GIS 3D map. This is due to the fact that the localization method unveils through experimentation provided earlier in the Section 3.1 that it is expected to have better accuracy when the receiver is placed at the center of the scatterers. It must be noted that although a near-perfect centered orientation and placement is ideal, the reality might be afar. Thus, the sensor positions should be perturbed (here set to $\pm 6^{\circ}$) for the scenarios to be realistic. Moreover, in order to simulate the problem geometry, the pulse width (τ) of the radar emitter was assumed to be 1μs. It was also considered that the receiver could estimate five distinct AOAs of radar signals with a certain measurement inaccuracy ($\gamma = \pm 3^{\circ}$). It should be noted that the angle of the incident ray was unaltered ($\gamma_0 = 90^{\circ}$).

Simulation setups were generated by changing the beamwidth (θ) of the radar emitter as 5° and 10°. Also, the radar emitter-receiver (r_0^o) distance was varied as 30 km, 40 km, and 50 km. For each scenario, pseudo-realistic terrain models were generated. In this way, unique pseudo-realistic scenes were achieved, each of which was defined by the beamwidth, the receiver placement, and the source-sink range. In each scene, both the receiver and the radar emitter were assumed to be placed on naval ships with their antennas at the height of 60 m. Besides, the height of the regions around the receiver varied between 250 and 450 m and spanned between 150 and 850 m at sea level. For each scenario, segmentation was performed by utilizing a DTED format level corresponding to a $25 \times 25m^2$ segment size. Hence, terrain data was then gathered to be used in the RT algorithm that calculates the PL values of the emitter-sensor-receiver links, which pave the way for calculating the probability of the scattering regions being a source of multipath signals accordingly. As a summary, the parameters employed for creating the simulation scenarios are listed in Table 3.1.

Simulations were then run on the pseudo-realistic scenes. After completing the simulations, the dataset containing the MSEs of the location estimates and the GDOP, along with the PL values obtained at 10^3 ensemble runs for a virtual sensor group, was created to be used in the ML experiments. In the created dataset, the PL values ranged from -70 dB to as high as -90 dB. On the other hand, based on its theory, the rating of GDOP values in the range between 1 and 10 is considered as relatively good, whereas the values in the range between 11 and 20 are fairly acceptable, and the values above 20 are an indication of poor localization geometry. As such, throughout the data

Table 3.1: Parameters of the simulation scenarios.

Parameter	Value
Pulsewidth (τ)	1μs
Frequency	9.4 GHz
Beamwidth (θ)	5°, 10° and 15°
Angle of Arrival (AOA) of the Direct Pulse	90°
Error in AOA Measurements (γ)	±3°
Number of Scatterer Regions (M)	4
GIS Resolution	DTED2 ($25m^2$)
Range (r_0^o)	30, 40, and 50 km
Antenna Heights	60 m
Height Span	[250, 450] m
Width Span	[150, 850] m
Perturbation Angle	±6°

acquisition phase, for the obtained virtual sensor groups, only the PL values that were below -90 dB and the GDOP values below 20 were utilized. As an example, in Table 3.2, a sample of the data collected for a virtual sensor group in a pseudo-realistic scene where $M = 4$ is given.

Table 3.2: Sample data ($M = 4$).

PLs of the Emitter-Scattering Center-Receiver Links (dB)				**GDOP**	**MSE** (dB)
Link 1	**Link 2**	**Link 3**	**Link 4**		
-84.642	-86.107	-80.506	-80.735	15.768	56.764
-77.193	-71.667	-79.369	-79.077	14.529	68.470
-78.050	-79.203	-77.799	-78.168	12.235	50.411
-76.009	-76.252	-77.127	-77.786	12.119	61.052
-74.128	-73.878	-73.633	-74.594	5.4540	56.263
-73.237	-76.801	-78.047	-77.681	16.343	57.091
-76.310	-75.394	-75.170	-74.876	8.8228	60.472
-70.099	-82.330	-75.907	-80.112	9.6142	43.705
-76.490	-79.590	-79.005	-73.002	7.1991	56.075
-72.123	-78.335	-79.211	-77.906	11.226	58.988

3.2.1.2 The Machine Learning Models

The created dataset is comprised of PL, GDOP, and MSE features that are well suited for the regression analysis that falls under supervised ML, which in turn lowers the computational requirements, unlike deep learning models, which may require

significantly higher computational resources. Therefore, as mentioned in Section 3.2, the regression ML models can be a good choice to enhance the radar emitter localization considered in this thesis. Among the popular regression ML models, Stepwise Linear Regression, Regression Tree, and NNs were chosen to be used in the experiments, be-cause of their distinguishable levels of complexity, which enables better analysis of the results. In the following, the selected regression ML models are briefly described.

3.2.1.2.1 Stepwise Regression

Linear regression models are typically characterized by predictors that exhibit linearity in relation to the model parameters. These models are known for their ease of interpretation and efficiency in making predictions. Among the various types of linear regression models, the commonly recognized ones include Linear, Interactions Linear, Robust Linear, and Stepwise Linear. For the purpose of this particular thesis, the Stepwise Linear Regression model was selected. This model employs stepwise regression techniques to construct a generalized linear model based on a given dataset. The stepwise regression process involves iteratively adding or removing predictors, starting from a constant model. It utilizes both forward and backward stepwise regression methods to determine the final model [120].

Prior to conducting the experiments, the initial conditions were established as Linear, implying the presence of constant and linear terms in the predictors. The upper limit, or the highest degree of terms that could be included in the model, encompassed constant, linear, and interaction terms among the predictors. Finally, the maximum number of steps imposed a constraint on the number of distinct linear models that could be tested during the stepwise procedure.

3.2.1.2.2 Regression Tree

The Regression Tree was selected as the second regression machine learning model. Specifically, it employed a decision tree algorithm with binary splits for regression purposes. Regression trees possess the advantages of being easily interpretable, efficient in terms of fitting and prediction, and requiring minimal memory usage. To avoid overfitting, it is advisable to cultivate smaller trees with fewer but larger leaves. Addi-

tionally, a greater number of smaller leaves leads to the creation of highly adaptable regression tree models [121].

In this thesiswork, a medium sized tree of 12 leaves was selected. Besides, since the created dataset had no missing data, accordingly there were no decision splits in the regression tree, the Surrogate Decision Splits feature was disabled before conducting the experiments.

3.2.1.2.3 Neural Network

Another model employed in the experiments was a NN-based regression model. Drawing inspiration from the human brain, a neural network is a flexible system that learns through interconnected nodes, or neurons, arranged in layers. By breaking down the input into layers of abstraction, a neural network effectively models non-linear relationships. These models are known for their strong predictive accuracy. Nevertheless, interpreting neural network models poses significant challenges. The model's adaptability grows with the inclusion of more fully connected layers in the network [122].

In addition to the input and output layers, the model used in the experiments had one hidden layer consisting of 100 neurons. Besides, the model had a linear output layer with one neuron. The activation function for the fully connected layer, excluding the output layer, was set to Rectified Linear Unit (ReLU). The regularization strength that specifies the ridge (L2) regularization penalty term was set to zero so that the sum of squared errors could be minimized. Data normalization was also enabled in order to center and scale each predictor to the corresponding mean and standard deviation.

As a summary, the ML models used in the experiments and their parameters are presented in Table 3.3.

3.2.1.3 Data Pre-processing and Training Details

The data format has crucial importance in ML applications for efficient training. In this context, it is known that normalizing the input data for the ML models enables the training phase to be accelerated. Feature normalization, in fact, affects the performance of a model. For instance, large-sized input data is expected to saturate the activation

Table 3.3: Machine learning models used in the experiments.

Models	Characteristics
Linear (Stepwise) Regression	Initial terms: Linear Upper bound: Interactions Max. num. steps: 1000
Decision Tree	Min. leaf size: 12 Surrogate decision splits: off
Neural Network	Fully connected layers: 1 First layer size: 100 Activation: ReLu Iteration limit: 1000 Regularization strength: 0 Standardize data: Yes

functions of the NN regression, including ReLu and Sigmoid, due to small (or no) feedback information.

In general, there are numerous normalization techniques that are widely used by data scientists and practitioners. These techniques are briefly described in the following sections. It is worthwhile to note that the generic symbols or variables are utilized in the formulation of the normalization techniques, which should not to be confused with those used in previous chapters.

One of the most popular normalization techniques is Z-normalization (or standardization). Assuming a dataset X consisting of N rows (entries) and D columns (features) such that $X[:, i]$ denotes the i-th feature and $X[j, :]$ is the entry j, the normalized data ($\hat{X}$) using Z-normalization can be computed as [123]

$$\hat{X}[:, i] = \frac{X[:, i] - \mu_i}{\sigma_i} , \tag{3.4}$$

where μ is the feature mean that can be calculated as

$$\mu_i = \frac{1}{N} \sum_{k=1}^{N} X[k, i] , \tag{3.5}$$

while σ is the feature standard deviation and calculated as

$$\sigma_i = \sqrt{\frac{1}{N-1}\sum_{k=1}^{N}(X[k,i]-\mu_i)}\,. \tag{3.6}$$

Although the Z-transformation does not change the distribution, it sets the mean to 0 and the standard deviation to 1. On the other hand, Min-Max normalization, which is the other popular normalization technique, simply allows to rescale the data in a range between 0 and 1 [123]. It can be formulated as

$$\hat{X}[:,i] = \frac{X[:,i] - \min(X[:,i])}{\max(X[:,i]) - \min(X[:,i])}\,. \tag{3.7}$$

Another common normalization technique is unit normalization, which scales the data such that the feature vector has a unit length [123]. It can be expressed as

$$\hat{X}[j,:] = \frac{X[j,:]}{\| X[j,:] \|}\,. \tag{3.8}$$

where $\| \cdot \|$ is the second norm operator.

The above-mentioned techniques tend to improve numerical stability and reduce training time in general. However, in some cases, normalization may not be desired due to the inherent properties of the features. For example, performance analysis may become difficult when straightforward reverse operations (de-normalization) are not easily attainable. Therefore, in this thesis, Min-Max normalization was utilized for the feature (input) set, including the PL and GDOP values, while leaving the MSE values in order to increase the model training speed and ease the model's learning evaluation.

Before conducting the experiments, a 5-fold cross-validation scheme was used to train the ML models. In the experiments, each of the models was trained on 2×10^6 randomly sampled data points from the respective pseudo-realistic scene datasets, while 10% of the data points were used for testing the performance of the models. The performance metric was the Root Mean Squared Error (RMSE), which is the standard deviation of the error term. Generally, the RMSE metric is frequently preferred, because of its alignment with the unit of the objective variable [124].

The summary of the trained ML models are given in Table 3.4. Note that average of the

experiment beamwidths (5°, 10°, and 15°) and ranges (30, 40, and 50 km) are presented here. Models were trained using a Workstation of the following specifications: two Intel® Xeon® Core™ E5-2680 28 Core CPU clocked at 2.40GHz with 176GB of RAM.

Table 3.4: Trained machine learning models' average characteristics.

Models	**Prediction Speed (obs/sec)**	**Training Time (min)**	**RMSE (dB)**
Linear (Stepwise) Regression	2.42×10^6	15.77	10.60
Decision Tree	7.42×10^5	92.31	9.37
Neural Network	9.13×10^5	262.95	10.48

As it can be seen that the linear model has the highest prediction speed compared to the other two due to having a lower complexity, which in turn results in a lowest prediction accuracy quantified by the RMSE. Similarly, the NN performs slightly better than the linear but has significantly larger training time (around 4 hours). Lastly, the Tree model has an acceptable training time of around 1.5 hours with the best accuracy.

3.2.1.4 Results

The results obtained from the experiments were evaluated in two steps. In the first step, it was aimed to assess the performance of the ML models presented in Section 3.2.1.2 on the dataset created for the simulation scenarios. A brief summary is tabularized in Table 3.4. To this end, the ML models were trained and tested on six datasets comprised of the data collected from the simulation scenarios. The RMSE of each model was then calculated for each of the scenarios. The average RMSEs of each model were calculated for six datasets. From the results, it was observed that the Decision Tree model reached the highest accuracy with an average RMSE of 9.37 dB. The stepwise regression and NN provided an average RMSE of 10.60 dB and 10.48 dB, respectively. Therefore, due to its lowest error, it was deduced that the Decision Tree model could be an efficient means to be used in the proposed localization approach.

In the second step, the accuracy of the proposed approach based on the Decision Tree algorithm was evaluated. In this context, the virtual sensor group that provided an optimal location estimate in terms of low MSE for each scenario was used in the

improved-TSWLS algorithm. Simulations were performed to obtain the MSEs of the location estimates by using Equation (3.1), where $L = 10^3$. Here, as described in [38, 39], the virtual sensor position noise power was determined as 6 dB in the implementation of the improved-TSWLS algorithm. The results obtained from the simulations were contrasted with the MSE estimates that were collected from the approach in [39] to assess the performance of the introduced approach. Moreover, the average computational (CPU elapsed) times were also compared to evaluate the time efficiency of the proposed approach. The results are listed in Table 3.5, where the computational times are given for a virtual sensor combination. Since, now we are closer to an actual deployable system, the localization runs were carried out in a commercially available laptop PC of the following specifications: Intel® Core™ i7-8750H 6 Cores CPU clocked at 2.20GHz with 16GB of RAM.

From the results listed in Table 3.5, it can be seen that the elapsed time of the proposed approach varies between about 23 and 28 *m*sec according to the localization scenario. However, the elapsed time of the method presented in [39] ranges from about 0.3 to 1.0 msec. It is important to note that the elapsed times are presented for only a single virtual sensor group. When all of the sensor combinations are considered, the elapsed time is expected to be greater than minutes or even hours. It is widely anticipated that the radar emitter will exhibit this behavior when it possesses a broad beam angle ($\theta \geq 10^\circ$). Then again, assuming abundant memory can be disposed for the system, often ML frameworks like MATLAB allows serializable queries to ML models. This in turn reduces the execution time substantially by keeping the query overheads to a minimum as tabulated in Table 3.6. The computation times across the datasets appear to vary quite a bit possibly due to MATLAB allocating resources and random processes engaging the CPU. Nevertheless, it is evident that the proposed approach exhibits significantly better performance in terms of elapsed time. Without any surprise, no performance gains are expected on the previous method in terms of execution time as that method is iterative in nature.

Regardless of the single or batch ML model query times, the proposed system visibly outperforms the previous approach as is suggested by the MSE values. Localization accuracy gains are comparatively less for narrower ($< 10^\circ$) beam angles than in wider ($\geq 10^\circ$) beamwidths.

Table 3.5: Comparisons of MSEs and computational times.

Dataset/ Scenario	**Proposed Approach**		**Previous Approach**	
	MSE (dB)	**Time** (ms)	**MSE** (dB)	**Time** (ms)
Dataset 1				
$\theta = 5°$	72.868	23.195	93.364	0.2979
$r_0^o = 30$ km				
Dataset 2				
$\theta = 5°$	77.257	27.082	95.166	0.3101
$r_0^o = 40$ km				
Dataset 3				
$\theta = 5°$	61.365	24.258	97.381	0.3061
$r_0^o = 50$ km				
Dataset 4				
$\theta = 10°$	50.756	26.526	92.558	0.4219
$r_0^o = 30$ km				
Dataset 5				
$\theta = 10°$	57.874	28.105	95.234	0.9907
$r_0^o = 40$ km				
Dataset 6				
$\theta = 10°$	52.456	23.877	97.008	0.3692
$r_0^o = 50$ km				
Dataset 7				
$\theta = 15°$	47.109	26.298	92.798	0.6927
$r_0^o = 30$ km				
Dataset 8				
$\theta = 15°$	52.779	24.191	95.098	0.4870
$r_0^o = 40$ km				
Dataset 9				
$\theta = 15°$	50.736	23.630	98.035	0.4543
$r_0^o = 50$ km				

Table 3.6: Proposed approach's average computational times.

Dataset/Scenario	Proposed Approach Average Time (μs)
Dataset 1 ($\theta = 5°, r_0^o = 30$ km)	4.315
Dataset 2 ($\theta = 5°, r_0^o = 40$ km)	0.152
Dataset 3 ($\theta = 5°, r_0^o = 50$ km)	0.281
Dataset 4 ($\theta = 10°, r_0^o = 30$ km)	0.367
Dataset 5 ($\theta = 10°, r_0^o = 40$ km)	0.170
Dataset 6 ($\theta = 10°, r_0^o = 50$ km)	0.145
Dataset 7 ($\theta = 15°, r_0^o = 30$ km)	0.186
Dataset 8 ($\theta = 15°, r_0^o = 40$ km)	1.121
Dataset 9 ($\theta = 15°, r_0^o = 50$ km)	1.278

3.2.1.5 Discussions

As discussed in [39], when the transmitter has a relatively large beamwidth, the widths of the scatterer regions become wider. The virtual sensor positions can then be obtained far from each other. In this case, higher localization accuracy is attainable by the localization method. Nevertheless, as a drawback, a large number of virtual sensors are expected to be obtained in wider scatterer regions. Besides, higher levels of DTED tiling schemes might also be desired for gathering more precise terrain data in practice. These issues may lead to a huge number of virtual sensors along with the PL values. Thus, the computational cost of the method becomes prohibitive. However, in this thesis, it is seen that faster computational time is possible when an ML-based approach is adopted in the localization process. Therefore, based on the experimental results, it is verified that the proposed approach is implementable in real-world applications if all operational requirements are satisfied. Yet, a large dataset containing useful features obtained from various operational conditions and environments is strictly required for proper implementation.

In the implementation of the proposed approach, it is imperative to utilize an efficient TDOA-based localization algorithm. In this thesis, improved TSWLS was used in order to properly compare the localization accuracies between the proposed approach and the existing method [39]. However, one of the current and efficient algorithms based on the TDOA measurements can be employed alternatively. This might also lead to a relatively higher level of localization accuracy.

On the other hand, based on the achieved experimental results, although all three of the regression models perform within a certain margin of error, the decision tree ML model is clearly the best choice, as it has reasonable prediction speed and a relatively low training time. In general, the traits of tree structures in ML are easy to interpret. Additionally, other advantages such as fast fitting and low memory usage make them an excellent mean when compared to Stepwise Linear Regression and NNs. It is worth mentioning that neural networks (NNs) are known for their strong predictive accuracy. However, when it comes to comprehending and elucidating the mechanisms behind these models, they tend to pose a greater level of difficulty. In this thesis, a feedforward fully connected NN was designed for regression. Results reveal that it is rather challenging to fine-tune a NN model. In this case, it only performs slightly better than the linear regression model while having a significantly longer training time. Then, the models are to be trained once and used for prediction multiple times for practical applications. Therefore, the training time may not be a deciding factor in choosing a model unless on-the-fly training is desired during deployment. Likewise, linear models are often easy to interpret and capable of making fast predictions. However, these models have rigid forms, and thus have low predictive accuracy. Even so, the applicability of such ML models requires further research to exhaust all other available options. For instance, other ML models like support vector machines, complex Tree structures, and deep NN could be investigated. In fact, the authors plan to explore such ML models in the near future. Another aspect that affects the feasibility of such systems is the accessibility of the actual ESM system. This would not only facilitate the production of such a system capable of passive localization using GIS data in a single receiver setup, but also allow real data from a real operational environment.

CHAPTER 4

ACCURACY ANALYSIS

This chapter is dedicated to extensive analysis of the results obtained in the Chapter 3. Apart from MSE as a performance metric, two more criteria are formulated and discussed to evaluate the proposed approach. In doing so, it should enable practitioners to gather further insights about the proposed data-driven passive localization system.

4.1 MSE Revisited

The proposed approach in section 3.2 outperforms the improved-TSWLS approach in [39]. This is illustrated in Figure 4.1 whose numeric values can be found in Table 3.6. Notice how the approach in [39] mimics the previous MSE trend for $> 10^{\circ}$ beamwidths across all ranges. On the other hand, the target estimation error is significantly reduced as is suggested by achieving a lower MSE. Additionally, the proposed data-driven approach saturates at higher beamwidths.

4.2 Circular Error Probable (CEP)

Circular Error Probable (CEP), which is another position accuracy analysis criterion, is sometimes preferred in EW. CEP is a unit of distance and can be thought of as a radius value at which the target location is the center. This circle contains half of all emission source locations detected. Alternatively, CEP radius is also known as the median error radius. Nonetheless, the CEP range will enable the performance evaluation from a different perspective. CEP is a well-known performance measure in ballistics and

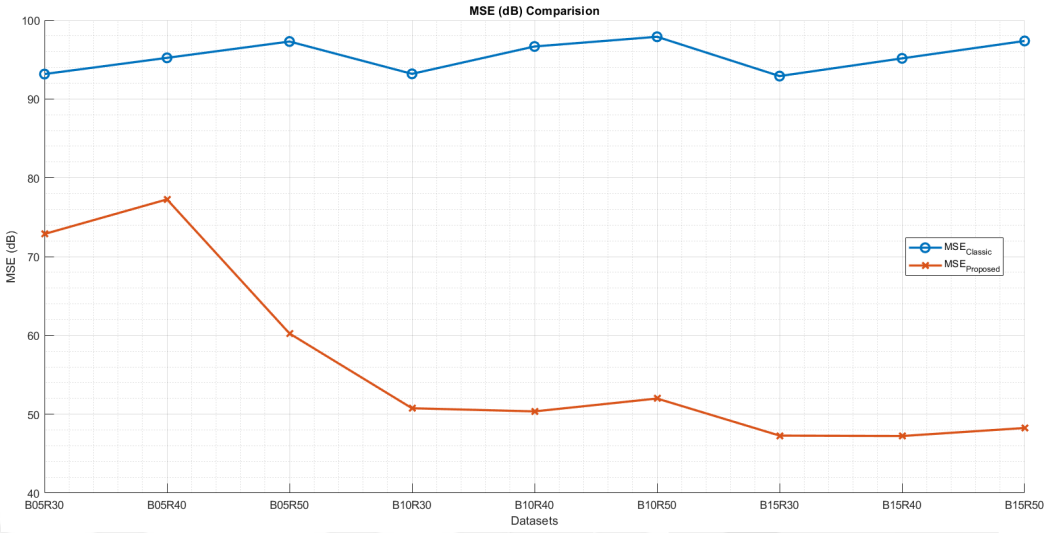

Figure 4.1: MSE comparison of the approaches.

navigation systems.

By definition, CEP is mathematically expressed as

$$\iint_{C_{CEP}} F(u,v)\,du\,dv = 0.5, \tag{4.1}$$

where u and v are the horizontal and the vertical errors, respectively, C_{CEP} is a circle centered at the target with radius CEP or mathematically put $u^2 + v^2 \leq CEP^2$, and $F(u,v)$ is a bivariate distribution function. Assuming a normal bivariate distribution, $F(u,v)$ can be expressed as

$$F(u,v) = \frac{1}{2\pi\sigma_u\sigma_v} e^{-\frac{1}{2}\left[\left(\frac{u}{\sigma_u}\right)^2 + \left(\frac{v}{\sigma_v}\right)^2\right]}, \tag{4.2}$$

Numerous CEP approximation techniques are present in the literature [125]. For simplicity, we will use the numerical method. The results are shown in the Figure 4.2. It can be seen that the proposed technique significantly lowers the bias compared to the previously published improved-TSWLS method.

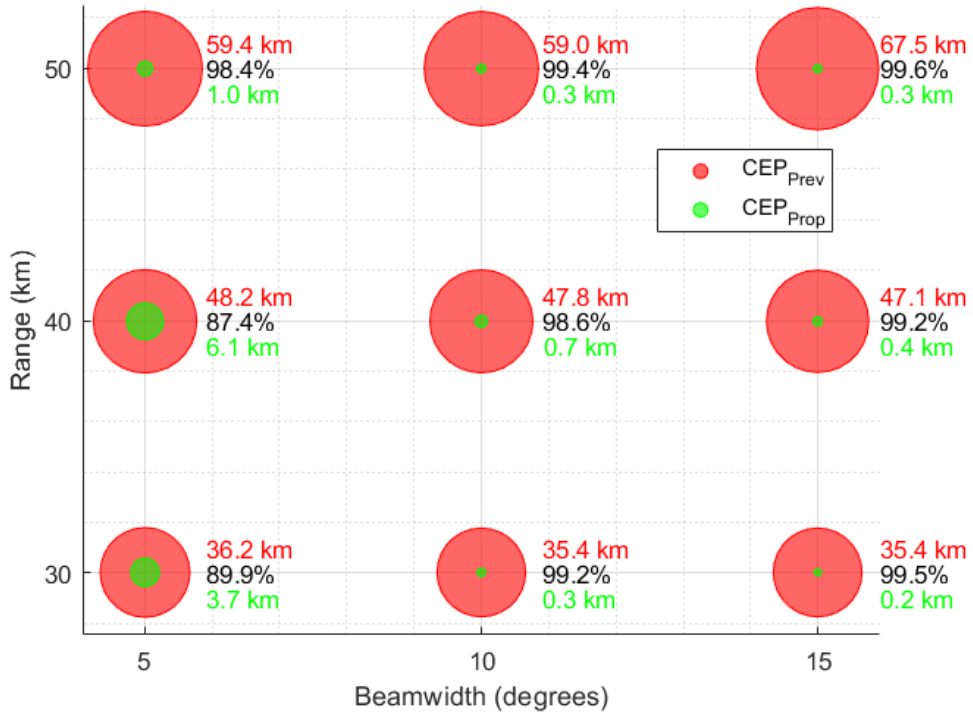

Figure 4.2: CEP comparison.

4.3 Spherical Error Probable (SEP)

The CEP Equation (4.1) presented earlier can be adopted for 3D accuracy analysis. Now, the 2D circle becomes a sphere and thus the name SEP. Hence, making it a volumetric integration over a trivariate distribution function as

$$\iiint_{V_{SEP}} F(u, v, w)\, du\, dv\, dw = 0.5. \tag{4.3}$$

Here, u, v and w are the x, y and z estimation errors, respectively. V_{SEP} is a sphere centered at the target with radius SEP given by $u^2 + v^2 + w^2 \leq SEP^2$. Lastly, $F(u, v, w)$ can be formulated as Equation 4.4 assuming a trivariate normal distribution function.

$$F(u, v, w) = \frac{1}{(2\pi)^{\frac{3}{2}}\sigma_u\sigma_v\sigma_w} e^{-\frac{1}{2}\left[\left(\frac{u}{\sigma_u}\right)^2+\left(\frac{v}{\sigma_v}\right)^2+\left(\frac{w}{\sigma_w}\right)^2\right]} \tag{4.4}$$

The SEP results computed using numeric integration are shown in the Figure 4.3. Similar to CEP, the proposed data-driven approach achieves a substantial smaller error probable radius in 3D.

4.4 Summary

At narrower beamwidths there are relatively smaller number of virtual sensors compared to the wider beams angles. This, in fact, impacts the learning degree of the data-driven approach. The behavior of estimation enhancement presented in Figure 4.1 is a indication of that. In other words, the MSE accuracy of the ML method is significantly improved for $< 10^\circ$ beam angles.

The proposed approach is also performant in terms of both CEP and SEP bias reduction. In fact, both (circular and spherical) error probable metrics reduced the area and the volume containing half the number of emitters respectively, by 96.79% on average. This translates to an average circular area of radius 1.4 km and an average spherical volume of 1.8 km approximately for the proposed method. Individual reduction rates are given in their respective figures above, for all the beamwidth-range combinations.

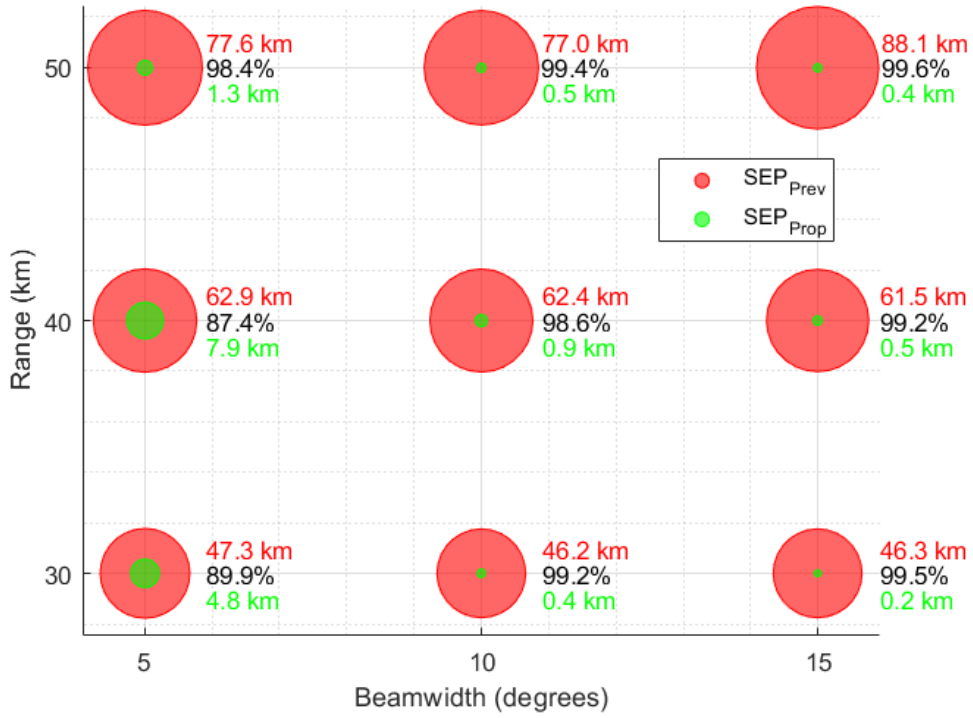

Figure 4.3: SEP comparison.

It is noteworthy that the percentage reduction is same for a particular scenario in both CEP and SEP, whereas the approximated radii are not. The proposed approach was capable of achieving as low as 200 meters in some scenarios.

CHAPTER 5

CONCLUSION

In this thesis, the effectiveness of a recently proposed emitter localization method, which relies on exploiting multipath, as discussed in [38], is assessed within realistic scenarios. The applicability and computational efficiency of the approach are examined by simulations conducted under various realistic scenarios. To do so, firstly the sensor position, orientation and geometry are investigated to uncover that a centered placement of the intercept receiver alone is capable of lowering the estimation error. Then, modern data-driven ML approaches are sought to further augment the accuracy of the passive location estimation system utilizing the multipath phenomena. As ML systems require large datasets, pseudo-realistic terrains were generated on which ample amount of tests were carried out to train ML systems.

Based on the findings, it can be inferred that the method's accuracy is deemed satisfactory in practical situations, making it highly feasible for implementation in the EW domain. Notably, placing the receiver at the center of the scatterers is anticipated to yield improved localization accuracy. Additionally, the method is projected to offer enhanced localization accuracy in scenarios with shorter distances. Furthermore, the results indicate that a wider beamwidth of the radar emitter ($\theta \geq 10^{\circ}$) is likely to result in better localization accuracy.

Conversely, the approach is projected to exhibit relatively inadequate performance in cases where the receiver is situated at the hind side of the sensor groups, and when the transmission source exhibits a tight beamwidth ($\theta < 10^{\circ}$). At present, the researchers are actively exploring innovative techniques to enhance the precision of the approach for these particular localization application use-cases.

Secondly, it can be verified that the proposed approach significantly reduces the computational time by escaping the inherent combinatorial complexity arising from virtual sensors. Hence, it becomes very useful for localization problems where the radar emitter exhibits a broad beamwidth ($\theta \geq 10^{\circ}$). Nevertheless, although the proposed approach is computationally efficient and provides accurate location estimates, the operational environment needs to be known a priori before implementation. Overall, it is believed that the results might provide some valuable insights on the use of ML in emitter localization.

Lastly, two more performance evaluation metrics, namely CEP and SEP, are investigated along with MSE. This allows interpretation of the proposed system from a different perspective with multiple criterion.

CHAPTER 6

FUTURE DIRECTIONS

In contrast to the more sophisticated ML models proposed in the literature, the ones introduced here are relatively simple. The literature suggests alternatives like Random Forest, eXtreme Gradient Boosting (XGB), and Support Vector Regression (SVR) for regression tasks, which are known for their superior performance. Moreover, Deep Learning techniques such as Deep Neural Network (DNN), Recurrent Neural Network (RNN), Long Short Term Memory (LSTM), and Convolutional Neural Network (CNN) are also recommended as more advanced options. Then again, complex models or more specifically deep neural networks are advisable and useful when the input parameters are around thousands. As a remedy, other aspects and performance metrics of the localization aspects can be incorporated in the future to increase the input set of parameters.

Although the proposed method works in an overall sense and better for larger beamwidths, intercept receivers having an operational beamwidth $\leq 10^{\circ}$ still requires more research and enhancements. Similarly, the range of a radar is capped by the operational environment and the theoretical maximum defined by the radio horizon. Therefore, more realistic ranges of parameters may be used.

As for the data acquisition technique, however novel it may be, prolonged data collection from actual deployment use cases is necessary for better training of ML models. Nonetheless, the pseudo-realistic model introduced in this paper serves as a basis for future works like radio coverage map researches and applications. Although there are some excellent publicly datasets for indoor and outdoor passive localization using inexpensive hardware using Wi-Fi, Bluetooth, SigFox, and Cellular, they are not usable

in the current context of outdoor multipath exploiting localization applications having ranges of tens of kilometers. On the other hand, actual radar data are proprietary and the radar itself is too expensive for most research centers. Thus, proper channels must be sought to acquire actual radar data.

In this paper, only four virtual sensors were assumed for a 3D emitter location estimation using TDOA. Further research is required to explore the effect of increasing the number of sensors on both the GDOP and the localization accuracy, and how to formulate a selection mechanism in cases where abundant or insufficient amount of sensors are present. Additionally, research directions towards combining multiple sensors might also be interesting.

REFERENCES

[1] Z. Sokol, J. Szturc, J. Orellana-Alvear, J. Popova, A. Jurczyk, and R. Célleri, "The role of weather radar in rainfall estimation and its application in meteorological and hydrological modelling—a review," *Remote Sensing*, vol. 13, no. 3, p. 351, 2021.

[2] S. Li, X. Gu, X. Xu, D. Xu, T. Zhang, Z. Liu, and Q. Dong, "Detection of concealed cracks from ground penetrating radar images based on deep learning algorithm," *Construction and Building Materials*, vol. 273, p. 121949, 2021.

[3] V. P. Tran, A. A. Al-Jumaily, and S. M. S. Islam, "Doppler radar-based non-contact health monitoring for obstructive sleep apnea diagnosis: A comprehensive review," *big data and cognitive computing*, vol. 3, no. 1, p. 3, 2019.

[4] C. Waldschmidt, J. Hasch, and W. Menzel, "Automotive radar—from first efforts to future systems," *IEEE Journal of Microwaves*, vol. 1, no. 1, pp. 135–148, 2021.

[5] G. Muntoni, G. Montisci, T. Pisanu, P. Andronico, and G. Valente, "Crowded space: a review on radar measurements for space debris monitoring and tracking," *Applied Sciences*, vol. 11, no. 4, p. 1364, 2021.

[6] C. Chang, A. Vadiraj, J. Bourassa, B. Balaji, and C. Wilson, "Quantum-enhanced noise radar," *Applied Physics Letters*, vol. 114, no. 11, 2019.

[7] M. Yaghi and M. Ö. Efe, "\text {H} _ {2}\text {/}\text {H} _ {\infty}-neural-based fopid controller applied for radar-guided missile," *IEEE Transactions on Industrial Electronics*, vol. 67, no. 6, pp. 4806–4814, 2019.

[8] J. A. López-Pastor, P. Arques-Lara, J. J. Franco-Peñaranda, A. J. García-Sánchez, and J. L. Gómez-Tornero, "Wi-fi rtt-based active monopulse radar for single access point localization," *IEEE Access*, vol. 9, pp. 34755–34766, 2021.

[9] S. Edstaller and D. Mueller, "A cooperative radar system with active reference target synchronization for kinematic target analysis," *IEEE Transactions on Microwave Theory and Techniques*, vol. 69, no. 9, pp. 4118–4131, 2021.

[10] H. Song, G. Wen, L. Zhu, and D. Li, "A novel tswls method for moving target localization in distributed mimo radar systems," *IEEE Communications Letters*, vol. 23, no. 12, pp. 2210–2214, 2019.

[11] J. Cong, X. Wang, X. Lan, M. Huang, and L. Wan, "Fast target localization method for fmcw mimo radar via vdsr neural network," *Remote Sensing*, vol. 13, no. 10, p. 1956, 2021.

[12] S. Li, Q. Zhang, B. Deng, B. Wu, and Y. Gao, "A fast and accurate leo satellite-based direct position determination assisted by tdoa measurements," *China Communications*, vol. 19, no. 1, pp. 92–103, 2022.

[13] Z. Wang, D. Hu, Y. Zhao, Z. Hu, and Z. Liu, "Real-time passive localization of tdoa via neural networks," *IEEE Communications Letters*, vol. 25, no. 10, pp. 3320–3324, 2021.

[14] L. Ai, M. Pang, C. Shan, C. Sun, Y. Kim, and B. Zhou, "A novel joint tdoa/fdoa passive localization scheme using interval intersection algorithm," *Information*, vol. 12, no. 9, p. 371, 2021.

[15] P. Wan, Q. Huang, G. Lu, J. Wang, Q. Yan, and Y. Chen, "Passive localization of signal source based on uavs in complex environment," *China Communications*, vol. 17, no. 2, pp. 107–116, 2020.

[16] K. C. Pine, S. Pine, and M. Cheney, "The geometry of far-field passive source localization with tdoa and fdoa," *IEEE Transactions on Aerospace and Electronic Systems*, vol. 57, no. 6, pp. 3782–3790, 2021.

[17] J. Li, S. Lv, Y. Liu, K. Zhang, L. Yang, and Y. He, "Performance analysis for space-air-ground integrated passive localization using TDOA measurements," in *2022 IEEE International Conference on Unmanned Systems (ICUS)*, IEEE, Oct. 2022.

[18] R. A. Khalil, N. Saeed, and M. Almutiry, "Uavs-assisted passive source localization using robust tdoa ranging for search and rescue," *ICT Express*, vol. 9, no. 4, pp. 677–682, 2023.

[19] Q. Li, B. Chen, and M. Yang, "Time difference of arrival passive localization sensor selection method based on tabu search," *Sensors*, vol. 20, no. 22, p. 6547, 2020.

[20] R. Poisel, *Electronic warfare target location methods*. Artech House, 2012.

[21] Y. Sun, K. Ho, and Q. Wan, "Solution and analysis of tdoa localization of a near or distant source in closed form," *IEEE Transactions on Signal Processing*, vol. 67, no. 2, pp. 320–335, 2018.

[22] Y. Sun, K. Ho, L. Gao, J. Zou, Y. Yang, and L. Chen, "Three dimensional source localization using arrival angles from linear arrays: Analytical investigation and optimal solution," *IEEE Transactions on Signal Processing*, vol. 70, pp. 1864–1879, 2022.

[23] T. Jia, H. Liu, K. Ho, and H. Wang, "Mitigating sensor motion effect for aoa and aoa-toa localizations in underwater environments," *IEEE Transactions on Wireless Communications*, 2023.

[24] C. Zhao and Y. Zhao, "One recurrent neural networks solution for passive localization," *Neural Processing Letters*, vol. 49, no. 2, pp. 787–796, 2019.

[25] S. Pak, B. K. Chalise, and B. Himed, "Target localization in multi-static passive radar systems with artificial neural networks," in *2019 International Radar Conference (RADAR)*, pp. 1–5, IEEE, 2019.

[26] H. Wu, Y. Cheng, and H. Wang, "Data-driven passive localization with non-cooperative radiation sources via mutually inverse networks," *IEEE Communications Letters*, vol. 24, no. 4, pp. 792–796, 2020.

[27] Y. Wang, Y. Wu, and Y. Shen, "Joint spatiotemporal multipath mitigation in large-scale array localization," *IEEE Transactions on Signal Processing*, vol. 67, no. 3, pp. 783–797, 2018.

[28] P. Zhang, D. Li, J. Zhao, and J. Cheng, "Multipath mitigation in gnss positioning by the dual-path compression estimation," *IEEE Sensors Journal*, vol. 20, no. 6, pp. 3087–3100, 2019.

[29] C. K. Seow and S. Y. Tan, "Localization of omni-directional mobile device in multipath environments," *Progress In Electromagnetics Research*, vol. 85, pp. 323–348, 2008.

[30] K. W. Lui and H. C. So, "Range-based source localisation with pure reflector in presence of multipath propagation," *Electronics Letters*, vol. 46, no. 13, pp. 957–958, 2010.

[31] C. S. Agate, M. Varble, and K. O. Ezal, "Ground-based emitter location in the presence of multipath," in *2019 IEEE Aerospace Conference*, pp. 1–8, IEEE, 2019.

[32] P. Setlur, G. E. Smith, F. Ahmad, and M. G. Amin, "Target localization with a single sensor via multipath exploitation," *IEEE Transactions on Aerospace and Electronic Systems*, vol. 48, no. 3, pp. 1996–2014, 2012.

[33] A. H. Muqaibel, M. G. Amin, F. Ahmad, *et al.*, "Target localization with a single antenna via directional multipath exploitation," *International Journal of Antennas and Propagation*, vol. 2015, 2015.

[34] A. O'connor, P. Setlur, and N. Devroye, "Single-sensor rf emitter localization based on multipath exploitation," *IEEE Transactions on Aerospace and Electronic Systems*, vol. 51, no. 3, pp. 1635–1651, 2015.

[35] R. Giacometti, A. Baussard, D. Jahan, C. Cornu, A. Khenchaf, and J.-M. Quellec, "Localization of radar emitters from a single sensor using multipath and tdoa-aoa measurements in a naval context," in *2016 24th European Signal Processing Conference (EUSIPCO)*, pp. 692–696, IEEE, 2016.

[36] M. Samizadeh Nikoo and F. Behnia, "Single-site source localisation using scattering data," *IET Radar, Sonar 0& Navigation*, vol. 12, no. 2, pp. 250–259, 2018.

[37] R. Ding, Z. Wang, L. Jiang, and S. Zheng, "Radar target localization with multipath exploitation in dense clutter environments," *Applied Sciences*, vol. 13, no. 4, p. 2032, 2023.

[38] Y. Dalveren and A. Kara, "Multipath exploitation in emitter localization for irregular terrains," *Radioengineering*, vol. 28, no. 2, 2019.

[39] M. A. Al Imran, E. Arık, Y. Dalveren, M. B. Tabakcioglu, and A. Kara, "On the accuracy of an emitter localization method based on multipath exploitation in realistic scenarios," *Journal of Electromagnetic Waves and Applications*, vol. 36, no. 15, pp. 2178–2197, 2022.

[40] M. N. de Sousa, R. L. Cardoso, H. S. Melo, J. W. Parente, and R. S. Thomä, "Machine learning and multipath fingerprints for emitter localization in urban scenario," in *Developments and Advances in Defense and Security: Proceedings of MICRADS 2019*, pp. 217–230, Springer, 2020.

[41] Y. Liu, F. Guo, L. Yang, and W. Jiang, "An improved algebraic solution for tdoa localization with sensor position errors," *IEEE Communications Letters*, vol. 19, no. 12, pp. 2218–2221, 2015.

[42] P. Meissner and K. Witrisal, "Multipath-assisted single-anchor indoor localization in an office environment," in *2012 19th International Conference on Systems, Signals and Image Processing (IWSSIP)*, pp. 22–25, IEEE, 2012.

[43] M. N. de Sousa and R. S. Thoma, "Single sensor rf emitter location using ray tracing multipath exploitation," in *2018 15th International Symposium on Wireless Communication Systems (ISWCS)*, pp. 1–6, IEEE, 2018.

[44] A. Abdallah and Z. Kassas, "Multipath mitigation via synthetic aperture beamforming for indoor and deep urban navigation," *IEEE Transactions on Vehicular Technology*, vol. 70, pp. 8838–8853, Sept. 2021.

[45] A. A. Abdallah and Z. M. Kassas, "Deep learning-aided spatial discrimination for multipath mitigation," in *2020 IEEE/ION Position, Location and Navigation Symposium (PLANS)*, IEEE, Apr. 2020.

[46] Z. Zhang, "Code and phase multipath mitigation by using the observation-domain parameterization and its application in five-frequency GNSS ambiguity resolution," *GPS Solutions*, vol. 25, Sept. 2021.

[47] Z. Wang, W. Chen, D. Dong, M. Wang, M. Cai, C. Yu, Z. Zheng, and M. Liu, "Multipath mitigation based on trend surface analysis applied to dual-antenna receiver with common clock," *GPS Solutions*, vol. 23, July 2019.

[48] P. Wang, Y. Wang, and Y. J. Morton, "Signal tracking algorithm with adaptive multipath mitigation and experimental results for LTE positioning receivers in urban environments," *IEEE Transactions on Aerospace and Electronic Systems*, vol. 58, pp. 2779–2795, Aug. 2022.

[49] Y. Tao, C. Liu, T. Chen, X. Zhao, C. Liu, H. Hu, T. Zhou, and H. Xin, "Real-time multipath mitigation in multi-GNSS short baseline positioning via CNN-LSTM method," *Mathematical Problems in Engineering*, vol. 2021, pp. 1–12, Jan. 2021.

[50] L. Benvenuto, T. Cosso, and G. Delzanno, "An adaptive algorithm for multipath mitigation in GNSS positioning with android smartphones," *Sensors*, vol. 22, p. 5790, Aug. 2022.

[51] C. Liu, Y. Tao, H. Xin, X. Zhao, C. Liu, H. Hu, and T. Zhou, "A single-difference multipath hemispherical map for multipath mitigation in BDS-2/BDS-3 short baseline positioning," *Remote Sensing*, vol. 13, p. 304, Jan. 2021.

[52] M. Mercuri, Y. Lu, S. Polito, F. Wieringa, Y.-H. Liu, A.-J. van der Veen, C. V. Hoof, and T. Torfs, "Enabling robust radar-based localization and vital signs

monitoring in multipath propagation environments," *IEEE Transactions on Biomedical Engineering*, vol. 68, pp. 3228–3240, Nov. 2021.

[53] E. I. P. Copa, K. Aziz, M. Rykunov, E. D. Greef, A. Bourdoux, and F. Horlin, "Radar fusion for multipath mitigation in indoor environments," in *2020 IEEE Radar Conference (RadarConf20)*, IEEE, Sept. 2020.

[54] Y. Wang, Y. Wu, and Y. Shen, "Joint spatiotemporal multipath mitigation in large-scale array localization," *IEEE Transactions on Signal Processing*, vol. 67, pp. 783–797, Feb. 2019.

[55] X. Zhang, L. Chen, M. Feng, and T. Jiang, "Toward reliable non-line-of-sight localization using multipath reflections," *Proceedings of the ACM on Interactive, Mobile, Wearable and Ubiquitous Technologies*, vol. 6, pp. 1–25, Mar. 2022.

[56] Z. Hao, H. Yan, X. Dang, Z. Ma, P. Jin, and W. Ke, "Millimeter-wave radar localization using indoor multipath effect," *Sensors*, vol. 22, p. 5671, July 2022.

[57] H. A. Nguyen, V. K. Nguyen, and K. Witrisal, "Amplitude modeling of specular multipath components for robust indoor localization," *Sensors*, vol. 22, p. 462, Jan. 2022.

[58] T. Wang, J. Liu, and Y. Shen, "A robust single-anchor localization method with multipath assistance in NLOS environments," in *2021 IEEE Global Communications Conference (GLOBECOM)*, IEEE, Dec. 2021.

[59] T. Wilding, E. Leitinger, and K. Witrisal, "Multipath-based localization and tracking considering off-body channel effects," in *2022 16th European Conference on Antennas and Propagation (EuCAP)*, IEEE, Mar. 2022.

[60] Z. Li, Z. Tian, W. Nie, and M. Zhou, "Configurable multipath-assisted indoor localization using active relay," *IEEE Transactions on Microwave Theory and Techniques*, vol. 70, pp. 155–168, Jan. 2022.

[61] H. Zhao, M. Huang, and Y. Shen, "High-accuracy localization in multipath environments via spatio-temporal feature tensorization," *IEEE Transactions on Wireless Communications*, vol. 21, pp. 10576–10591, Dec. 2022.

[62] Z. Xu, C. Fan, and X. Huang, "MIMO radar waveform design for multipath exploitation," *IEEE Transactions on Signal Processing*, vol. 69, pp. 5359–5371, 2021.

[63] Y. Rong, A. Aubry, A. D. Maio, and M. Tang, "Diffuse multipath exploitation for adaptive detection of range distributed targets," *IEEE Transactions on Signal Processing*, vol. 68, pp. 1197–1212, 2020.

[64] U. Kumbul and H. T. Hayvaci, "Multipath exploitation for knowledge-aided adaptive target detection," *IET Radar, Sonar & Navigation*, vol. 13, pp. 863–870, June 2019.

[65] Y. Dalveren and A. Kara, "Multipath exploitation in emitter localization for irregular terrains," *Radioengineering*, vol. 27, pp. 473–482, June 2019.

[66] P. Zhang, G. Li, C. Huo, and H. Yin, "Exploitation of multipath micro-doppler signatures for drone classification," *IET Radar, Sonar & Navigation*, vol. 14, pp. 586–592, Apr. 2020.

[67] D. L. Hall, R. M. Narayanan, and D. M. Jenkins, "SDR based indoor beacon localization using 3d probabilistic multipath exploitation and deep learning," *Electronics*, vol. 8, p. 1323, Nov. 2019.

[68] R. Feng, E. D. Greef, M. Rykunov, H. Sahli, S. Pollin, and A. Bourdoux, "Multipath ghost recognition for indoor MIMO radar," *IEEE Transactions on Geoscience and Remote Sensing*, vol. 60, pp. 1–10, 2022.

[69] Z. Zhang, B. Chen, and M. Yang, "Moving target detection based on time reversal in a multipath environment," *IEEE Transactions on Aerospace and Electronic Systems*, vol. 57, pp. 3221–3236, Oct. 2021.

[70] M. A. A. Imran, E. Arık, Y. Dalveren, M. B. Tabakcioglu, and A. Kara, "On the accuracy of an emitter localization method based on multipath exploitation in realistic scenarios," *Journal of Electromagnetic Waves and Applications*, vol. 36, pp. 2178–2197, May 2022.

[71] M. A. Alsheikh, S. Lin, D. Niyato, and H.-P. Tan, "Machine learning in wireless sensor networks: Algorithms, strategies, and applications," *IEEE Communications Surveys & Tutorials*, vol. 16, no. 4, pp. 1996–2018, 2014.

[72] D. Burghal, A. T. Ravi, V. Rao, A. A. Alghafis, and A. F. Molisch, "A comprehensive survey of machine learning based localization with wireless signals," 2020.

[73] Z. Li, K. Xu, H. Wang, Y. Zhao, X. Wang, and M. Shen, "Machine-learning-based positioning: A survey and future directions," *IEEE Network*, vol. 33, pp. 96–101, May 2019.

[74] P. Roy and C. Chowdhury, "A survey of machine learning techniques for indoor localization and navigation systems," *Journal of Intelligent & Robotic Systems*, vol. 101, Mar. 2021.

[75] A. Nessa, B. Adhikari, F. Hussain, and X. N. Fernando, "A survey of machine learning for indoor positioning," *IEEE Access*, vol. 8, pp. 214945–214965, 2020.

[76] P. Yadav and S. C. Sharma, "A systematic review of localization in WSN: Machine learning and optimization-based approaches," *International Journal of Communication Systems*, vol. 36, Nov. 2022.

[77] T. Yang, A. Cabani, and H. Chafouk, "A survey of recent indoor localization scenarios and methodologies," *Sensors*, vol. 21, p. 8086, Dec. 2021.

[78] P. S. Bithas, E. T. Michailidis, N. Nomikos, D. Vouyioukas, and A. G. Kanatas, "A survey on machine-learning techniques for UAV-based communications," *Sensors*, vol. 19, p. 5170, Nov. 2019.

[79] V. Bellavista-Parent, J. Torres-Sospedra, and A. Pérez-Navarro, "Comprehensive analysis of applied machine learning in indoor positioning based on wi-fi: An extended systematic review," *Sensors*, vol. 22, p. 4622, June 2022.

[80] C. Wu, H. Hou, W. Wang, Q. Huang, and X. Gao, "TDOA based indoor positioning with NLOS identification by machine learning," in *2018 10th International Conference on Wireless Communications and Signal Processing (WCSP)*, IEEE, Oct. 2018.

[81] M. N. de Sousa and R. S. Thoma, "Applying random forest and multipath fingerprints to enhance TDOA localization systems," *IEEE Antennas and Wireless Propagation Letters*, vol. 18, pp. 2316–2320, Nov. 2019.

[82] M. N. de Sousa and R. S. T. Electronic, "Enhanced localization systems with multipath fingerprints and machine learning," in *2019 IEEE 30th Annual International Symposium on Personal, Indoor and Mobile Radio Communications (PIMRC)*, IEEE, Sept. 2019.

[83] M. N. de Sousa and R. S. Thomä, "Enhancement of localization systems in NLOS urban scenario with multipath ray tracing fingerprints and machine learning," *Sensors*, vol. 18, p. 4073, Nov. 2018.

[84] M. N. D. Sousa and R. S. Thoma, "Mobile station localization emitter in urban NLoS using multipath ray tracing fingerprints and machine learning," in *2018 8th International Conference on Localization and GNSS (ICL-GNSS)*, IEEE, June 2018.

[85] J. He and H. C. So, "A hybrid TDOA-fingerprinting-based localization system for LTE network," *IEEE Sensors Journal*, vol. 20, pp. 13653–13665, Nov. 2020.

[86] F. Carrino, A. Janka, O. A. Khaled, and E. Mugellini, "LoRaLoc: Machine learning-based fingerprinting for outdoor geolocation using LoRa," in *2019 6th Swiss Conference on Data Science (SDS)*, IEEE, June 2019.

[87] A. Niitsoo, T. Edelhausser, and C. Mutschler, "Convolutional neural networks for position estimation in TDoA-based locating systems," in *2018 International Conference on Indoor Positioning and Indoor Navigation (IPIN)*, IEEE, Sept. 2018.

[88] B. Ma, C. Tong, L. Zou, and M. Tian, "A TDOA localization method for complex environment localization," *Journal of Physics: Conference Series*, vol. 2004, p. 012003, Aug. 2021.

[89] C. Xu, Z. Wang, Y. Wang, Z. Wang, and L. Yu, "Three passive TDOA-AOA receivers based flying-UAV positioning in extreme environments," *IEEE Sensors Journal*, pp. 1–1, 2020.

[90] M. N. de Sousa, R. L. Cardoso, H. S. Melo, J. W. C. Parente, and R. S. Thomä, "Machine learning and multipath fingerprints for emitter localization in urban scenario," in *Smart Innovation, Systems and Technologies*, pp. 217–230, Springer Singapore, June 2019.

[91] L. Polka, C. Balanis, and A. Polycarpou, "High-frequency methods for multiple diffraction modeling: Application and comparison," *Journal of electromagnetic waves and applications*, vol. 8, no. 9-10, pp. 1223–1246, 1994.

[92] K.-Y. Kam, L.-Y. Chew, and L.-W. Li, "Multipath propagation of radio waves in 3-dimensional terrains," *Journal of electromagnetic waves and applications*, vol. 15, no. 3, pp. 411–431, 2001.

[93] M. Tabakcioglu and A. Kara, "Comparison of improved slope uniform theory of diffraction with some geometrical optic and physical optic methods for multiple building diffractions," *Electromagnetics*, vol. 29, no. 4, pp. 303–320, 2009.

[94] M. B. Tabakcioglu and A. Kara, "Improvements on slope diffraction for multiple wedges," *Electromagnetics*, vol. 30, no. 3, pp. 285–296, 2010.

[95] M. B. Tabakcioglu, "S-utd-ch model in multiple diffractions," *International Journal of Electronics*, vol. 103, no. 5, pp. 765–774, 2016.

[96] K. Rizk, R. Valenzuela, D. Chizhik, and F. Gardiol, "Application of the slope diffraction method for urban microwave propagation prediction," in *VTC'98. 48th IEEE Vehicular Technology Conference. Pathway to Global Wireless Revolution (Cat. No. 98CH36151)*, vol. 2, pp. 1150–1155, IEEE, 1998.

[97] R. G. Kouyoumjian and P. H. Pathak, "A uniform geometrical theory of diffraction for an edge in a perfectly conducting surface," *Proceedings of the IEEE*, vol. 62, no. 11, pp. 1448–1461, 1974.

[98] C. Tzaras and S. R. Saunders, "An improved heuristic utd solution for multiple-edge transition zone diffraction," *IEEE Transactions on Antennas and Propagation*, vol. 49, no. 12, pp. 1678–1682, 2001.

[99] D. A. McNamara, C. W. Pistorius, and J. Malherbe, "Introduction to the uniform geometrical theory of diffraction," *(No Title)*, 1990.

[100] Y. Dalveren and A. Kara, "Comparative analysis of tdoa-based localization methods in the presence of sensor position errors," in *2017 4th International Conference on Control, Decision and Information Technologies (CoDIT)*, pp. 0556–0560, IEEE, 2017.

[101] K. S. Trivedi, *Probability & statistics with reliability, queuing and computer science applications*. John Wiley & Sons, 2008.

[102] Y.-P. Lei, F.-X. Gong, and Y.-Q. Ma, "Optimal distribution for four-station tdoa location system," in *2010 3rd International Conference on Biomedical Engineering and Informatics*, vol. 7, pp. 2858–2862, IEEE, 2010.

[103] Z. Dai, G. Wang, X. Jin, and X. Lou, "Nearly optimal sensor selection for tdoa-based source localization in wireless sensor networks," *IEEE transactions on vehicular technology*, vol. 69, no. 10, pp. 12031–12042, 2020.

[104] Y. Zhao, Z. Li, B. Hao, P. Wan, and L. Wang, "How to select the best sensors for tdoa and tdoa/aoa localization?," *China Communications*, vol. 16, no. 2, pp. 134–145, 2019.

[105] I. Sharp, K. Yu, and Y. J. Guo, "Gdop analysis for positioning system design," *IEEE Transactions on Vehicular Technology*, vol. 58, no. 7, pp. 3371–3382, 2009.

[106] C.-S. Chen, Y.-J. Chiu, C.-T. Lee, J.-M. Lin, *et al.*, "Calculation of weighted geometric dilution of precision," *Journal of Applied Mathematics*, vol. 2013, 2013.

[107] K. Ho, X. Lu, and L.-o. Kovavisaruch, "Source localization using tdoa and fdoa measurements in the presence of receiver location errors: Analysis and solution," *IEEE Transactions on Signal Processing*, vol. 55, no. 2, pp. 684–696, 2007.

[108] N. Levanon, "Lowest gdop in 2-d scenarios," *IEE Proceedings-radar, sonar and navigation*, vol. 147, no. 3, pp. 149–155, 2000.

[109] M. N. de Sousa, R. Sant'Ana, R. P. Fernandes, J. C. Duarte, J. A. Apolinário, and R. S. Thomä, "Improving the performance of a radio-frequency localization system in adverse outdoor applications," *EURASIP Journal on Wireless Communications and Networking*, vol. 2021, no. 1, pp. 1–26, 2021.

[110] M. N. de Sousa and R. S. Thomä, "Applying random forest and multipath fingerprints to enhance tdoa localization systems," *IEEE Antennas and Wireless Propagation Letters*, vol. 18, no. 11, pp. 2316–2320, 2019.

[111] F. Bao, S. Mazokha, and J. O. Hallstrom, "Mobintel: Passive outdoor localization via rssi and machine learning," in *2021 17th International Conference on Wireless and Mobile Computing, Networking and Communications (WiMob)*, pp. 247–252, IEEE, 2021.

[112] D. Dogan, Y. Dalveren, and A. Kara, "A mini-review on radio frequency fingerprinting localization in outdoor environments: Recent advances and challenges," in *2022 14th International Conference on Communications (COMM)*, pp. 1–5, IEEE, 2022.

[113] Ç. Yapar, R. Levie, G. Kutyniok, and G. Caire, "Real-time outdoor localization using radio maps: A deep learning approach," *IEEE Transactions on Wireless Communications*, 2023.

[114] M. A. Alsheikh, S. Lin, D. Niyato, and H.-P. Tan, "Machine learning in wireless sensor networks: Algorithms, strategies, and applications," *IEEE Communications Surveys & Tutorials*, vol. 16, no. 4, pp. 1996–2018, 2014.

[115] Z. Deng, H. Wang, X. Zheng, and L. Yin, "Base station selection for hybrid tdoa/rtt/doa positioning in mixed los/nlos environment," *Sensors*, vol. 20, no. 15, p. 4132, 2020.

[116] J. Lu, L. Ye, and S. Han, "Analysis and application of geometric dilution of precision based on altitude-assisted ins/sar integrated navigation," *IEEE Transactions on Instrumentation and Measurement*, vol. 70, pp. 1–10, 2020.

[117] L. Polok, R. Barton, P. Chudy, P. Krsek, P. Smrz, and D. Petr, "Terrain rendering algorithm performance analysis," in *2012 IEEE/AIAA 31st Digital Avionics Systems Conference (DASC)*, pp. 2E3–1, IEEE, 2012.

[118] J. J. Scott and N. A. Dodgson, "Example-based terrain synthesis with pit removal," *Computers & Graphics*, vol. 99, pp. 43–53, 2021.

[119] V. Le Chevalier, M. Jaeger, X. Mei, A. Lesluye, and P.-H. Cournède, "A functional landscape prototype to simulate water resource competition between plants," in *2006 Second International Symposium on Plant Growth Modeling and Applications*, pp. 124–134, IEEE, 2006.

[120] M. A. Efroymson, "Multiple regression analysis," *Mathematical methods for digital computers*, pp. 191–203, 1960.

[121] L. Breiman, J. Friedman, C. J. Stone, and R. A. Olshen, *Classification and regression trees*. CRC press, 1984.

[122] T. L. Fine, *Feedforward neural network methodology*. Springer Science & Business Media, 2006.

[123] A. Zheng and A. Casari, *Feature engineering for machine learning: principles and techniques for data scientists*. " O'Reilly Media, Inc.", 2018.

[124] A. Botchkarev, "Performance metrics (error measures) in machine learning regression, forecasting and prognostics: Properties and typology," *arXiv preprint arXiv:1809.03006*, 2018.

[125] Y. Wang, G. Yang, D. Yan, Y. Wang, and X. Song, "Comprehensive assessment algorithm for calculating cep of positioning accuracy," *Measurement*, vol. 47, pp. 255–263, 2014.